**Energy &
Environmental
Science**

Material and system development needs for widespread deployment of hydroxide exchange membrane fuel cells in light-duty vehicles

**SCHOLARONE™
Manuscripts**

Broader context

Hydroxide exchange membrane fuel cell (HEMFC) offers cost savings over proton exchange membrane fuel cell (PEMFC) in stack component materials. The performance and durability of HEMFC have been dramatically improved, and the electrochemically-driven CO_2 separator (EDCS) has addressed the CO_2-induced voltage-loss problems. HEMFC has reached a point where it can be seriously considered for deployment in light-duty vehicle (LDV) applications. One of the critical remaining issues is determining the system cost of HEMFC LDVs, as the widespread commercialization of HEMFC LDVs depends on cost parity with internal combustion engine vehicles. Here, we determine and analyze the cost of HEMFC systems for LDV applications for the first time by developing a comprehensive system model. We also determine the material and system developments needed to decrease the HEMFC system cost to the US Department of Energy's ultimate cost target of 30 $/kW$_{Net}$ at a large production volume of 500,000 systems/year, which enables cost parity with internal combustion engines. Overall, our work informs the future materials and system component developments by identifying the highest cost and voltage-loss drivers in HEMFC systems and the relative importance of EDCS operating parameters.

Material and system development needs for widespread deployment of hydroxide exchange membrane fuel cells in light-duty vehicles

Author Names: Reza Abbasi[*], Brian P. Setzler, and Yushan Yan[*]

Affiliation(s): Center for Clean Hydrogen and Department of Chemical and Biomolecular Engineering, University of Delaware, 150 Academy Street, Newark, DE 19716, USA

[*]Corresponding Author E-mail Address: Reza Abbasi: (abbasi@udel.edu; abbasi2@wisc.edu)

Yushan Yan: (yanys@udel.edu)

Abstract

Hydroxide exchange membrane fuel cell (HEMFC) is a promising alternative to proton exchange membrane fuel cell (PEMFC) and offers cost savings in stack component materials. In this study, we determine and analyze the cost of HEMFC systems for light-duty vehicle applications for the first time by developing a comprehensive HEMFC system model. More specifically, (i) We analyze the volumetric and cost-based activity of state-of-the-art carbon-supported precious metal (PM)-containing and PM-free oxygen reduction reaction (ORR) and hydrogen oxidation reaction (HOR) electrocatalysts. Incorporating the activity of the ORR-HOR electrocatalyst pairs into the HEMFC system cost analysis, we conclude that PM-containing PdMo/C and Ru_7Ni_3/C are the best ORR and HOR electrocatalysts for implementation in HEMFC systems; (ii) We perform a HEMFC system cost analysis based on the best state-of-the-art carbon-supported PM-free ORR-HOR electrocatalyst pair ((Fe-N-C)-Ni/N-doped C). We also compare the system cost of HEMFC and PEMFC based on the best state-of-the-art carbon-supported ORR and HOR electrocatalysts. Our comparison shows that

the HEMFC system has a cheaper stack but a more expensive balance of plant (BOP) than PEMFC, resulting in a higher HEMFC system cost. The higher HEMFC system cost is due to the electrochemically-driven CO_2 separator (EDCS) cost and higher humidification management system cost caused by the lower cathode outlet relative humidity of HEMFC compared with that of PEMFC; (iii) We determine the material and system developments needed to decrease the HEMFC system cost to $30/kW_{Net}$ required for cost competitiveness with internal combustion engine vehicles (ICEVs) based on (PdMo/C-Ru_7Ni_3/C) and ((Fe-N-C)-Ni/N-doped C) ORR-HOR electrocatalyst pairs. We also perform a single variable sensitivity analysis and demonstrate the relative importance of EDCS operating parameters: H_2 consumed to CO_2 removed ratio, pressure drop, and area-based cost. Our analysis indicates that EDCS pressure drop significantly impacts the overall HEMFC system cost, comparable to the area-based cost, and that one must monitor its values in future studies; and (iv) We present a detailed stack and BOP cost and voltage-loss breakdown for all the systems studied in this paper and identify the cost and voltage-loss drivers. Overall, our system analysis provides invaluable and transformational guidelines and enables more targeted and informed future materials and system component developments by identifying the highest cost and voltage-loss drivers in HEMFC systems and providing material and system developments needed to reach full cost parity with ICEVs.

Broader context

Hydroxide exchange membrane fuel cell (HEMFC) offers cost savings over proton exchange membrane fuel cell (PEMFC) in stack component materials. The performance and durability of HEMFC have been dramatically improved, and the electrochemically-driven CO_2

separator (EDCS) has addressed the CO_2-induced voltage-loss problems. HEMFC has reached a point where it can be seriously considered for deployment in light-duty vehicle (LDV) applications. One of the critical remaining issues is determining the system cost of HEMFC LDVs, as the widespread commercialization of HEMFC LDVs depends on cost parity with internal combustion engine vehicles. Here, we determine and analyze the cost of HEMFC systems for LDV applications for the first time by developing a comprehensive system model. We also determine the material and system developments needed to decrease the HEMFC system cost to the US Department of Energy's ultimate cost target of 30 $/kW$_{Net}$ at a large production volume of 500,000 systems/year, which enables cost parity with internal combustion engines. Overall, our work informs the future materials and system component developments by identifying the highest cost and voltage-loss drivers in HEMFC systems and the relative importance of EDCS operating parameters.

Introduction

Proton exchange membrane fuel cell (PEMFC) is a promising alternative power source for light-duty vehicles (LDVs) because it uses hydrogen as a fuel, which can be produced from clean-energy resources such as solar and wind.[1-3] In addition, PEMFC has high fuel-to-energy conversion efficiency and zero tailpipe emissions.[1, 2] PEMFCs have reached such a level of technology readiness that several prominent automotive companies are either producing or planning to produce thousands to tens of thousands of PEMFC LDVs per year.[1, 2, 4, 5]

Hydroxide exchange membrane fuel cell (HEMFC) is an alternative to PEMFC, which offers a potential pathway to cost savings in stack component materials.[6] The significant research interest in HEMFC stems from a multitude of reasons. First, the alkaline environment

of HEMFC is much less corrosive compared to the acidic environment of PEMFC. The less

corrosive environment enables the use of non-precious metal (PM) electrocatalysts.[6-10] It also

opens the possibility of designing new classes of superior PM-containing electrocatalysts that

are either alloyed or modified with non-PM elements that would otherwise be inherently

unstable in the acidic environment of PEMFC.[11] Second, the high-pH and less corrosive

environment of HEMFC also enables the use of cheaper substrate metals like aluminum for

bipolar plates (BPPs), and it removes the need for PM-containing BPP coatings that are

currently used in PEMFCs.[1, 2, 6] Finally, most of the high-performance hydroxide exchange

ionomers (HEIs) presently used in the hydroxide exchange membranes (HEMs) and HEMFC

electrodes are hydrocarbon-based.[3, 7, 9, 12-16] These HEIs are generally expected to be cheaper

and safer to make than perfluorinated sulfonic acid (PFSA) proton exchange ionomers (PEIs)

currently used in proton exchange membranes (PEMs) and electrodes of the state-of-the-art

PEMFCs.[1, 2, 6]

Early research and development of HEMFCs were significantly hindered by low

performance, with typical power densities well below 0.5 W/cm^2 and poor durability.[17-19] For

some years, the combination of low achievable power densities and poor durability made

HEMFCs uncompetitive with PEMFCs. However, over the past few years, outstanding

progress has been made in improving HEMFC performance[6, 7, 9, 12, 13, 15, 16, 20] and durability[7,

13]. Current state-of-the-art high-performance HEMFCs have achieved power density values

over 3 W/cm^2 operating with CO_2-free H_2/O_2 gas feeds. [12, 13, 16] They have also achieved a

power density value of around 1.75 W/cm^2 working with CO_2-free H_2/air gas feeds.[13] Similarly,

the durability of HEMFCs has improved significantly.[7, 13, 21] Of particular interest, recently,

Mustain and coworkers developed a high-performance HEMFC that achieved record-setting durability at a current density of 600 mA/cm^2 for 2000 h using PM electrocatalysts both at the anode (PtRu/C; PM loading=0.7 mg/cm^2) and cathode electrodes (Pt/C; PM loading=0.6 mg/cm^2).[13] The HEMFC showed an outstanding ultra-low voltage degradation rate of 15.36 µV/h, resulting in only 3.65% voltage degradation over the 2000 h durability test.[13]

Another critical and long-recognized practical hurdle for implementing HEMFCs in real-world applications has been the profound negative impact of CO_2 on the performance of HEMFCs.[6, 22-24] Excellent recent experimental[24] and modeling[22] efforts have elucidated and deconvoluted the root causes of increased voltage losses in the presence of CO_2. The consensus achieved in the HEMFC community is that using atmospheric air containing >400 ppm CO_2 as the cathode feed can easily result in intolerable cell voltage loss of 150 to 400 mV, depending on the HEMFC operating conditions.[22-24] Consequently, from an operational perspective in real-world applications such as LDVs, sustained operation in air containing >400 ppm CO_2 requires HEMFC system designs incorporating CO_2 scrubbing of air to an acceptable single-digit ppm CO_2 concentration before the air is fed to an operating HEMFC.[6, 22, 23]

Significant progress has been made in tackling the problem of CO_2 by developing and successfully demonstrating an electrochemically-driven CO_2 separator (EDCS) unit.[23, 25, 26] Within a HEMFC operating with CO_2-contanining cathode air feed, CO_2 dissolves readily into the aqueous environment at the cathode. Subsequently, it reacts with hydroxide (OH^-) to produce carbonate (CO_3^{-2}) and bicarbonate (HCO_3^-). The OH^-, CO_3^{-2}, and HCO_3^- are then transported across the HEM to the anode of HEMFC, where CO_3^{-2}, and HCO_3^- accumulate until the local anode pH is lowered enough for the CO_2 evolution reactions to happen.[23, 25, 26] The

EDCS system has been developed based on the idea of using the undesirable side reactions

with CO_2 in a HEMFC to capture CO_2, and the EDCS unit is basically a small HEMFC unit

optimized for CO_2 removal placed upstream of a HEMFC stack on the cathode side, scrubbing

atmospheric air to an acceptable single-digit ppm CO_2 concentration.[23, 25, 26] EDCS operates at

a much lower current density than a HEMFC, and its H_2 consumption can be satisfied using

the purged H_2 from the HEMFC stack rather than fresh H_2 from the H_2 fuel tank.[23, 25, 26] The

idea of EDCS has been demonstrated successfully, and EDCS units have already shown

excellent CO_2 separation efficacy at low H_2 consumption levels.[23, 25, 26] In addition, EDCS units

have been coupled successfully with HEMFCs enabling the use of CO_2-containing ambient air

as feed for an operating HEMFC with minimal CO_2-related voltage degradation.[23]

Early demonstrations of EDCS used fuel cell (FC) components such as BPPs, current

collectors, and load control systems.[23, 25, 26] These components make scaling up the EDCS and

integrating it in a HEMFC LDV system challenging, considering the volume and cost

limitations required by the LDV applications.[23, 25, 26] This challenge has been addressed

adequately by successfully demonstrating a shorted membrane EDCS that removes CO_2 from

the air feed using a carbon-containing HEM that conducts both electrons and anions.[26] The

shorted membrane EDCS could remove >99% CO_2 from the air feed to a downstream HEMFC

stack with a small H_2 consumption of <2% of that of the HEMFC stack during a continuous

450 h operation, with a slight average rise of CO_2 concentration of about six ppb/h in the EDCS

air exhaust stream.[26] The shorted membrane EDCS could also operate effectively in dynamic

conditions, and tuning the rate of H_2 supply effectively controlled the current in the EDCS,

eliminating the need for load control systems.[26] Finally, as the shorted membrane EDCS did

not use FC components such as BPPs, current collectors, and load control systems, it could be easily scaled to a compact spiral-wound module.[26] A prototype spiral-wound EDCS module achieved one-pass 98% CO_2 removal during a continuous 80 h operation.[26]

Overall, the results of the above studies show that the performance and durability of HEMFCs have been significantly improved and that EDCS has been demonstrated as a successful way of addressing the CO_2 problem. Therefore, we are now at a point in HEMFC research and development (R&D) where the future deployment of HEMFCs for real-world applications such as LDVs is a serious consideration. Consequently, the time has come to contemplate and answer some of the remaining issues that the HEMFC researchers have mostly neglected until now. One of the most critical remaining issues is determining the system cost of HEMFC for LDVs. The widespread commercialization of HEMFC for LDVs ultimately depends on the economic competition with the incumbent and advanced internal combustion engine vehicles.[1, 2, 6] To this end, the US Department of Energy (DOE) has set an ultimate system cost target of 30 $/kW$_{Net}$ for FC-based LDVs at a large production volume of 500,000 systems/year, which enables reaching full cost parity with internal combustion engine vehicles.[1, 2, 6] A clear testament to the significance of tracking the system cost of FC-based LDVs is the continuous support, funding, and emphasis devoted by the DOE to analyze, baseline, and track the system cost of PEMFC for LDVs.[1, 2, 6] A similar effort to determine the system cost of HEMFC for LDVs does not exist. Performing this system cost analysis is of utmost importance for the HEMFC research community as it identifies cost drivers, which subsequently allows allocating HEMFC R&D efforts most efficiently toward the most significant cost drivers.[1, 2]

Following the above-described logic, this paper aims to determine and analyze the cost of

HEMFC systems for LDV applications for the first time and answer some fundamentally and

technologically essential questions regarding the HEMFC systems, as detailed below. We have

organized this paper into four sections. The first section describes a comprehensive FC system

model we developed for LDV applications. This system includes a pseudo-two-dimensional

(pseudo-2-D) FC stack, an EDCS unit, an air management system, a thermal management

system, a humidification management system, a fuel management system, and additional

balance of plant (BOP) components (Figure 1). In the second section, we describe the details

of our FC system cost estimation approach. In addition, we explain how we determined the

total FC system cost based on the currently available oxygen reduction reaction (ORR) and

hydrogen oxidation reaction (HOR) electrocatalysts. And subsequently, we explain how we

determine the material and system developments needed to achieve the FC system cost target

of 30 $/kW$_{Net}$. In the third section, we analyze the volumetric and cost-based activity of state-

of-the-art carbon-supported PM-containing and PM-free ORR and HOR electrocatalysts.

When combined with HEMFC system cost analysis for ORR-HOR electrocatalyst pairs, our

analysis demonstrates that PM-containing PdMo/C and Ru$_7$Ni$_3$/C are the best ORR and HOR

electrocatalysts for implementation in HEMFC systems. Due to significant research interest in

developing entirely PM-free HEMFC systems,[6] we also perform a HEMFC system cost

analysis based on the best state-of-the-art carbon-supported PM-free ORR-HOR electrocatalyst

pair ((Fe-N-C)-Ni/N-doped C). In addition, we compare the system cost of PEMFC and

HEMFC based on the best state-of-the-art carbon-supported ORR and HOR electrocatalysts.

Our comparison shows that the HEMFC system has a cheaper stack but a more expensive BOP

than PEMFC, resulting in a higher HEMFC system cost. This higher HEMFC system cost is mainly due to the EDCS cost and higher humidification management system cost caused by the lower cathode outlet relative humidity (RH) of HEMFC compared with that of PEMFC. Finally, we present a detailed stack and BOP cost and voltage-loss breakdown for the systems studies in this section. In the fourth section, we determine the material and system developments needed to decrease the HEMFC system cost to $30/kW_{Net} required for cost competitiveness with internal combustion engine vehicles based on $PdMo/C-Ru_7Ni_3/C$ and (Fe-N-C)-Ni/N-doped C ORR-HOR electrocatalyst pairs. This section also presents a detailed stack and BOP cost and voltage-loss breakdown for these two systems. Furthermore, in this section, we perform a single variable sensitivity analysis and demonstrate the relative importance of operating parameters of EDCS, namely H_2 consumed to CO_2 removed ratio, pressure drop, and area-based cost. Our analysis indicates that EDCS pressure drop significantly impacts the overall system cost, comparable to the area-based cost, and that one must monitor its values in future studies. Overall, our work provides transformational guidelines and allows more targeted future materials and system component developments by identifying the highest cost and voltage-loss drivers in HEMFC systems and the relative importance of EDCS operating parameters.

Description of FC system model for LDV applications

The architectural features of HEMFCs are similar to those of PEMFCs, and the main difference lies in the FC chemistry. PEMFCs operate in an acidic environment. In contrast, HEMFCs operate in an alkaline environment.[6, 22] Consequently, we adopted the PEMFC system configuration presented in the Strategic Analysis Inc. (SA) comprehensive report,

prepared under the guidance of DOE for an 80 kW$_{Net}$ PEMFC system.[1] We updated it to match

the requirements of a HEMFC system by adding an EDCS unit upstream of the HEMFC stack

on the cathode side (Figure 1). Subsequently, we developed a comprehensive system model for

LDV applications. As discussed in detail below, our system includes a pseudo-2-D FC stack,

an EDCS unit, an air management system, a humidification management system, a thermal

management system, a fuel management system, and additional BOP components. Based on

the directions provided by DOE, we did not include the compressed H$_2$ tank and its accessories,

LDV battery, electric traction motor, traction inverter module, and the rest of the LDV,

including the frame, body, interior of LDV, or its comfort-related features such as driver's

instruments, seats, and windows in the technoeconomic analysis of LDV system.[1, 2]

FC stack performance model

Technoeconomic analysis of FC systems for LDV applications corresponds to nominal

high-power density events of LDVs, where the FC stack must deliver 80 kW$_{Net}$ power to the

LDV traction motor.[1] These events, according to General Motors (GM) and SA comprehensive

report, correspond to a FC stack operating at high temperature (95 °C), high reactant utilization

operating conditions (H$_2$ stoichiometry=1.5 and O$_2$ stoichiometry=1.5), and inlet anode and

cathode of 65% RH.[1, 27] According to the SA report, single cells are assembled in series in the

FC stack to deliver a system voltage of 250 V required for compatibility with the LDV electric

traction motor.[1]

Like the SA report, we adopted a hierarchical approach to building our FC stack based on

a single cell.[1] The inlet gases in the FC stack are distributed to every cell via a manifold. We

assumed uniform inlet gas distribution such that inlet gases are equally distributed among all

cells. We also assumed that all the cells in the FC stack are the same and perform the same. Consequently, a single-cell model can stand for the whole stack, and the stack current would be equal to a single-cell current, and the stack voltage would be equal to the number of the single cells multiplied by the operation voltage of a single cell.[1]

We modeled a single cell operating in a counter-flow mode in the FC stack using a pseudo-2-D FC model based on the excellent FC modeling framework already available in the literature.[22] A pseudo-2-D FC model is a one-dimensional (1-D) FC sandwich model coupled with a 1-D down-the-channel model and treats a single cell operating in counter-flow mode as several differential units that come from the discretization of the single cell along the flow direction. Each discretization unit of a single cell acts like a FC operating under "differential" conditions (i.e., constant species' partial pressures and constant total pressure in the anode and cathode flow channels) and is modeled using a 1-D FC sandwich model. The discretization units communicate via a 1-D down-the-channel model that considers the variations in gaseous species' partial pressures and total pressure in the anode and cathode flow channels.

The 1-D FC sandwich model only considers the direction normal to the membrane electrode assembly (MEA) along the MEA thickness. It includes two gas diffusion layers (GDLs), two microporous layers (MPLs), two electrocatalyst layers, and a membrane. The 1-D FC sandwich model considers species transport in gas, current flow in the electronically conducting phase, ion transport in the ionomer within membrane and electrodes, water transport in the ionomer within membrane and electrodes, accurate description of the stoichiometry and kinetics of electrochemical reactions, and heat transfer. Of particular note, the 1-D FC sandwich model fully implements the effect of O_2 and H_2 cross-over, electro-

osmotic drag, and local-O_2 transport resistance resulting from the O_2 transport through the ionomer in the cathode electrocatalyst layer. In addition, the 1-D FC sandwich model neglects H_2O condensation within the MEA.

The 1-D down-the-channel model consists of mass balance down the channel for the species in the channel coupled with an assumption of linear total pressure drop along the flow channel. We also applied a proper correction term to account for the single-cell voltage loss resulting from the buildup of N_2 in the recirculating anode gas in FC stacks of LDVs. Figure S1 in the electronic supporting information (ESI) shows the schematic of our pseudo-2-D FC model, and we included more details about our modeling approach in the ESI.

We validated our 1-D FC sandwich model and pseudo-2-D FC model by comparing their results with benchmark PEMFC experimental polarization curves provided by GM for cells operating in either differential mode (5 cm² active area single cell) or counter-flow mode (50 cm² active area single cell).[27] The electrocatalysts in these PEMFCs are supported on high surface area carbon (HSC). Figure 2 compares the experimental polarization curve with the model polarization curve for PtCo/HSC cathode (Pt loadings=0.2 mg$_{Pt}$/cm²) coupled with Pt/HSC anode (Pt loadings=0.025 mg$_{Pt}$/cm²) for PEMFCs operating either in differential mode or counter-flow mode. We included similar comparisons for two other PtCo/HSC cathodes at different Pt loadings (0.1 and 0.05 mg$_{Pt}$/cm²) coupled with Pt/HSC anode (Pt loadings=0.025 mg$_{Pt}$/cm²) in the ESI (Figures S3 and S4). Close inspection of Figures 2, S3, and S4 shows that the overall agreement between polarization curves produced by our 1-D FC sandwich model or our pseudo-2-D FC model and the GM's benchmark experimental ones is very reasonable. After validating our model, we made the required changes in the electro-osmotic drag and

stoichiometry and kinetics of electrochemical reactions to capture the underlying physics of HEMFCs accurately. We used this HEMFC model to predict the performance of the HEMFC stack (see the ESI for more details). Our model also allows a detailed voltage-loss breakdown analysis enabling us to determine the voltage-loss drivers at the operating conditions of the stack. We included the mathematical definition of each voltage-loss term in the ESI.

FC stack cost model

The Hydrogen and Fuel Cell Technologies Office of DOE manages multiple projects that estimate the cost of various FC and hydrogen production technologies.[1] In 2018, the office directed that all cost-estimating projects report costs using the same basis year dollars (2016 $) to enable meaningful and informative comparison of the expenses between various FC and hydrogen production technologies.[1] SA accommodated this request in 2018 and made all the required cost adjustments by using the ratio of the Producer Price Index (PPI) for finished goods published by the Bureau of Labor Statistics for July 2016 and July 2018 to adjust the cost values to 2016 $.[1, 28] Consequently, all the cost of materials values and the cost models for the stack and BOP available in the SA report are in 2016 $ values.

We adopted the cost models for the stack and BOP presented in the SA report for the PEMFC LDV system.[1] We updated them as needed to reflect the HEMFC stack and BOP cost by applying proper correction terms to the cost models. When required, we characterized the cost of materials used in the cost models/correction terms by the commodity price of the content of metals. As directed by SA, we kept the Pt cost constant at 1500 $/tr.oz in 2016 dollars.[1] For all PMs except Pt, we used the prices provided by Johnson Matthey at the end of January 2022 and then converted the costs into 2016 dollars using the ratio of PPI for finished goods for July

2016 and January 2022.[28, 29] For non-precious metals, we used the prices provided by the London Metal Exchange at the end of January 2022 and then converted the costs into 2016 dollars using the ratio of PPI for finished goods for July 2016 and January 2022.[28, 30] The only exception to this approach involved estimating the material cost of the Fe-N-C electrocatalyst. The 2015 SA report provides a cost estimation for a Polyaniline-Iron-Carbon (PANI)-based Fe-N-C electrocatalyst produced at large scales for a large production volume of 500,000 LDV systems/year.[31] We adopted this cost and converted it into 2016 dollars using the ratio of PPI for finished goods for July 2016 and December 2015 and then used it in our cost estimation. Overall, all cost values in this paper are in 2016 dollars.

The SA report provides a PEMFC stack cost model that we adopted and updated by applying some corrections to the cost model to reflect the HEMFC stack's cost.[1] First, we changed the BPP from 316L stainless steel coated with PM-containing TreadStone DOTS-R coating to aluminum coated with TreadStone TiO_X-containing coating, which is PM-free.[1] Next, we replaced the PFSA PEI in the membrane and electrodes with a cheaper HEI that had the same ionic conductivity and H_2O permeability as 700 equivalent weight (EW) PFSA. Using the stack cost model and cost information provided in the SA report,[1] we performed a component cost breakdown and separated the stack cost into the following component costs: anode/cathode electrocatalyst cost, expanded polytetrafluoroethylene (ePTFE) membrane substrate cost, total ionomer within electrodes and membrane cost, BPP cost, GDL coated with MPL cost, subgasket and its sealing cost, and balance of stack (BOS) cost. We included more details about our approach in the ESI.

EDCS performance and cost model

In our HEMFC system for LDVs, we incorporated an EDCS unit upstream of the HEMFC stack on the cathode side, which scrubs CO_2 from the atmospheric air reducing its concentration from 420 ppm to 4 ppm (Figure 1). We envisioned our EDCS to be a shorted membrane EDCS with a spiral-wound structure similar to that described in our previous work.[26] In a spiral-wound structure, the electrocatalyst-covered membrane is packaged into a spiral-wound module with a high area-to-volume ratio and compactness. Consequently, the volume of the EDCS unit will be reasonable for implementation in a HEMFC-based LDV.[26] Inside the EDCS, H_2 reacts with O_2, which produces H_2O and heat.[23, 25, 26] If left unmanaged, the heat released in the EDCS unit can result in significant temperature increases within the unit, quickly degrading the ionomer in the membrane and electrodes. Unlike the FC stack, the shorted membrane EDCS with a spiral-wound structure has no cooling cells in its construction.[26] Consequently, we decided to add a heat management strategy where a pump injects the liquid H_2O gathered in the anode demister into the anode flow in the EDCS (Figure 1). A portion of that liquid H_2O will evaporate and enable the isothermal operation of the EDCS. This evaporated H_2O will end up in the airflow of the EDCS due to its higher flow rate. We also assumed intermittent electrochemical purges would be applied to the HEMFC stack at the time of refueling of the LDV.[26] These considerations mean that the negative impact of CO_2 on the HEMFC performance is mitigated.[26] We chose the concentration of 4 ppm as the EDCS outlet CO_2 concentration, as it allows a reasonable time interval between the intermittent electrochemical purges of the HEMFC stack, comparable to the time interval between the refueling of a FC-based vehicle with a vehicle driving range of about 650 km (2021 Toyota Mirai XLE48).[26]

Using our previous EDCS performance modeling efforts,[25] we developed a detailed EDCS performance model that allows calculating the required EDCS active area. Using our previous EDCS cost estimation efforts,[26] we created an updated cost model for the EDCS that allows calculating the EDCS cost from the required EDCS active area and the area-based cost of EDCS. We included more details about our EDCS performance modeling and cost estimation approach in the ESI.

Air management system performance and cost model

According to the SA report, the air management system includes six components: 1) Air filter and housing, 2) Air mass flow sensor, 3) Integrated air compressor, expander, and motor with a motor controller unit (CEM), 4) Air temperature sensor, 5) Stack inlet/stack outlet manifold for the air stream and air ducting, and 6) Demister (Figure 1).[1] The CEM unit is based on a Honeywell design and includes a centrifugal compressor, a radial-inflow expander, and an electric motor with a motor controller.[1] The centrifugal compressor consumes power to provide airflow at desired pressures. The radial-inflow expander that produces power from the air stream exiting the FC stack and the electric motor with a motor controller, which receives power from the FC stack, drive the centrifugal compressor.[1]

We developed a detailed performance model for the CEM unit based on the information provided in the SA report, which allowed us to calculate the power requirement of the electric motor of the CEM unit.[1] We adopted the air management system cost model provided in the SA report, and we updated it by applying some corrections to the cost model.[1] First, the cost model does not incorporate the scenario where the FC system does not need an expander (i.e. when the air stream enters the expander at atmospheric pressure). We included this scenario in

the cost model by applying a suitable correction term based on the information provided in the SA report.[1] Next, for our 30 \$/kW$_{Net}$ LDV systems, we used a cost correction term consistent with the cost reduction in the CEM unit cost outlined in the SA report, which is expected to be achieved in the future through engineering and scientific research and innovation.[1] We included more details about our air management system performance and cost estimation approach in the ESI.

Humidification management system performance and cost model

According to the SA report, the humidification management system includes 1) An air pre-cooler and 2) A membrane humidifier (Figure 1).[1] The air pre-cooler sits between the centrifugal compressor and the membrane humidifier, cooling the hot compressed air exiting the compressor to the stack's operating temperature (95 °C). The humidifier is a cross-flow membrane humidifier in which streams of dry air from the air pre-cooler outlet and humid, O$_2$-depleted air from the FC cathode outlet exchange water through the membrane. Since the mass transfer in a cross-flow membrane humidifier is conceptually quite similar to heat transfer in a cross-flow heat exchanger, we used the cross-flow heat exchanger modeling framework available in the literature to develop a performance model for the cross-flow membrane humidifier. The SA report provides a humidification management system cost model, and we adopted this cost model for our cost estimation.[1] We included more details about our humidification management system performance and cost estimation approach in the ESI.

Thermal management system cost model and calculating the parasitic power requirements of its components

According to the SA report, the thermal management system includes two coolant loops: 1) A high-temperature coolant loop (HTCL) and 2) A low-temperature coolant loop (LTCL).[1] The HTCL cools the FC stack and consists of a coolant reservoir, a coolant pump, a coolant resin deionizer (DI) filter, coolant piping, a thermostat & valve, a radiator, and a radiator fan (Figure 1).[1] The LTCL cools the motor of the CEM unit, the electronic components of the CEM unit, and the compressed air intake in the air pre-cooler before it goes into the membrane humidifier.[1] The LTCL consists of a coolant reservoir, a coolant pump, coolant piping, a thermostat & valve, and a radiator (Figure 1).[1] The SA report provides a thermal management system cost model, and we adopted this cost model for our cost estimation.[1] The thermal management system includes a HTCL pump, a HTCL radiator fan, and a LTCL pump whose operation requires receiving power from the FC stack.[1] We developed a model that allowed us to calculate the parasitic power requirements of these components based on the information provided in the SA report.[1] We included more details about our thermal management system cost model and the calculation of the parasitic power requirements of the HTCL pump, the HTCL radiator fan, and the LTCL pump in the ESI.

Fuel management system description and cost model

According to the SA report, the fuel management system includes five components: 1) Two injectors: injector A is for the regular operation of the FC stack, and injector B enables purge events, 2) A pressure transducer (PT), 3) A pulsed ejector that enables H_2 recirculation from the anode exhaust to the anode inlet, 4) Three valves: an overpressure cut-off valve that

is included in fuel loop as a safety precaution to prevent accidental FC stack pressurization from the high pressure in the H_2 storage tank, a check valve to ensure that H_2 does not flow backward from the pulsed ejector, and a purge valve that allows for periodic purging of the H_2 in the fuel loop and 5) H_2 inlet and outlet of stack manifolds and H_2 piping (Figure 1).[1] The fuel management system has a constant cost of \$213.09 \$/system ($C_{Fuel} = 213.09$ \$).[1]

Additional BOP components description and cost model

According to the SA report, the additional BOP components include four items: 1) A system controller; 2) All FC system sensors except those that were included as a part of the air management system; 3) Miscellaneous BOP components, including FC stack belly pan, H_2/air mixer, mounting frames, wiring, and fasteners for wiring & piping; and 4) FC system assembly and testing.[1] The cost of additional BOP components is constant (368.58 \$/system; $C_{BOP,Additional} = 368.58$ \$).[1]

Details of the FC system cost estimation approach

We can calculate the total FC system cost for the LDV (C_{System}; \$) from the FC stack cost (C_{Stack}; \$), EDCS unit cost (C_{EDCS}; \$), air management system cost (C_{Air}; \$), humidification management system cost (C_{Humid}; \$), the thermal management system's cost ($C_{Thermal}$; \$), the fuel management system cost (C_{Fuel}; \$), and the cost of additional BOP components ($C_{BOP,Additional}$; \$) as presented in equation 1.

$$C_{System} = C_{Stack} + C_{EDCS} + C_{Air} + C_{Humid} + C_{Thermal} + C_{Fuel} + C_{BOP,Additional} \quad (1)$$

We explained in detail in the previous section and the ESI how to calculate all the cost components of C_{System}. One can convert C_{System} and all its cost components into a (\$/kW$_{Net}$)

basis by simply dividing the costs by the net power requirement of the FC-based LDV (80 kW_{Net}).[1] The FC stack operating parameters are: 1) The stack inlet pressure, which is the same for the anode and cathode inlets (P_{Inlet}^{Stack}); 2) Cathode and anode electrocatalyst loadings ($L_{Cathode}$ and L_{Anode}), or equivalently the thickness of the cathode and anode electrocatalyst layers (t_{ACL} and t_{CCL}); and 3) The operating voltage of a single cell in the FC stack (V_{Cell}).[1] The FC stack is the critical component within the FC system, and the operating parameters of the FC stack effectively dictate all the cost components of C_{System} except C_{Fuel} and $C_{BOP,Additional}$.[1]

The operation of a FC system for a LDV is subject to three critical constraints.[1] First, the BOP of the FC system includes some key components whose operation requires receiving power from the FC stack. These components include the electric motor of the CEM unit, the HTCL pump, the HTCL radiator fan, the LTCL pump, and components such as the FC system controller and sensors.[1] In addition to providing the parasitic power requirements of these components, the FC stack has to deliver 80 kW of power to the electric traction motor of the LDV that drives the vehicle wheels.[1] Second, for compatibility with the electric traction motor of the LDV, the FC stack must deliver a system voltage of 250 V.[1] Finally, the size of the radiator rejecting waste heat to ambient should be reasonable for incorporation into a light-duty automobile.[1] We included a detailed discussion of how we implemented these constraints in our system model in the ESI.

A multi-variable global optimization approach determines the total FC system cost for the LDV and the FC stack operating conditions.[1] In this approach, the objective function (i.e., the function that we want to minimize) is the total FC system cost, and the free variables of

optimization (i.e., the variables that define the search space of the optimization) are the FC stack operating parameters.[1] We optimized the total FC system cost in MATLAB using the Genetic Algorithm (GA) method, a global optimization algorithm inspired by natural selection, evolution, and genetics concepts.[32, 33] The GA method is inspired by Charles Robert Darwin's "Survival of the Fittest" theory. The GA method starts with a randomly generated population of solutions for a global optimization problem. Each solution in the population is then assigned a fitness value based on its objective function value, and the solutions with lower objective function values acquire better fitness values. Subsequently, consistent with the "Survival of the Fittest" theory, fitter solutions are given a higher chance to evolve and yield even more "fitter" solutions. The solutions in the population then undergo evolutionary processes of recombination and mutation (like in natural genetics), producing new solutions, and the process is repeated over various generations until the fittest solution is found (we refer the interested readers to the excellent references available in the literature for more details on how GA method operates).[32, 33] We selected the GA method for optimizing the total FC system cost for two reasons: i) GA method does not require any derivative information of the objective function, and consequently, it is faster and more robust as compared to traditional gradient-based optimization methods; and ii) The GA method has excellent parallel computation capabilities and can run exceptionally fast on multi-core computers.[32, 33]

Details of determining the total FC system cost based on currently available ORR and HOR electrocatalysts

The free variables of global optimization are the FC stack operating parameters.[1] We must assign a range to these parameters to perform the global optimization.

P_{Inlet}^{Stack} range: We assigned a lower bound of 1.31 atm and a higher bound of 2.5 atm to P_{Inlet}^{Stack}. As discussed in the ESI, the lower bound of 1.31 atm corresponds to a scenario where the pressure of the airstream entering the expander equals the atmospheric pressure. We chose the higher bound of 2.5 atm because it corresponds to the FC stack inlet pressure of the 2018 LDV PEMFC system described in the SA report.[1]

t_{CCL} range: For the HEMFC systems, where we incorporated PdMo/C as the ORR electrocatalyst, and for the PEMFC system, where we incorporated Pt_3NiMo/C as the ORR electrocatalyst, we assigned a lower bound of 1 μm and a higher bound of 60 μm to t_{CCL}. For the HEMFC system, where we incorporated Fe-N-C as the ORR electrocatalyst, we assigned a lower bound of 1 μm and a higher bound of 132.5 μm to t_{CCL}. We assigned a larger value to the higher bound of t_{CCL} for Fe-N-C because, as we will see later, the ORR volumetric activity of Fe-N-C is significantly lower than PdMo/C and Pt_3NiMo/C.

t_{ACL} range: For the HEMFC systems, where we incorporated Ru_7Ni_3/C, Ni/N-doped C, and PtRu/C as the HOR electrocatalysts, we assigned a lower bound of 1 μm and a higher bound of 60 μm to t_{ACL}. For the PEMFC system, where we incorporated Pt/C as the HOR electrocatalyst, we assigned a lower bound of 1 μm and a higher bound of 20 μm to t_{ACL}. We assigned a smaller value to the higher bound of t_{ACL} for Pt/C because, as we will see later, the HOR volumetric activity of Pt/C in acidic electrolyte is higher than all the state-of-the-art carbon-supported PM-containing and PM-free HOR electrocatalysts in alkaline electrolyte.

V_{Cell} range: We assigned a lower bound of 0.64 V and a higher bound of 0.9 V to V_{Cell}.

As discussed in the ESI, our pseudo-2-D FC model corresponds to a FC operating in counter-flow mode. In this operation mode, the anode gas channel exit is adjacent to the cathode gas channel inlet, and the anode gas channel inlet is adjacent to the cathode gas channel exit (Figure S1). Since we do not know the exit conditions of the anode/cathode gas channels a priori, solving the pseudo-2-D FC model requires an elaborative and very time-consuming iterative guess and check approach. In this approach, we guessed the cell average current density and the exit composition of the anode gas channel. Subsequently, we ran the pseudo-2-D FC model iteratively, renewing the guessed values several times until the inlet conditions of the anode gas channel and anode/cathode calculated stoichiometry matched the known values. We note that independent of the global optimization method (e.g., GA method, simulated annealing) that one chooses for a complex multi-variable optimization problem like the one considered here, finding the global optimum requires a large number of accurate and undisrupted computations of the objective function, which makes using the pseudo-2-D FC model impractical for the optimization purpose.[32-35] We note that a FC polarization curve acquired using a 1-D FC sandwich model that operates based on the average of the inlet and exit pressure and composition of the anode and cathode gas channels is a reasonable surrogate for the FC polarization curve acquired using a pseudo-2-D FC model. Consequently, we optimized the total FC system cost using the below-described multi-step approach.

1. We calculated a reasonable estimate for the exit RH of the anode and cathode gas channels using the pseudo-2-D FC model for a FC operating with reasonable operating parameters inspired by the 2018 LDV PEMFC system described in the SA report. We described these FC operating parameters below.

1.1 We assigned the values of P_{Inlet}^{Stack} and V_{Cell} to be the same as the values of P_{Inlet}^{Stack}

and V_{Cell} of the 2018 LDV PEMFC system ($P_{Inlet}^{Stack} = 2.5\ atm$ and V_{Cell}

$= 0.657\ atm$).[1]

1.2 We set t_{CCL} for the FC systems that incorporated PM-containing ORR electrocatalysts

using the cathode Pt loading of the 2018 LDV PEMFC system (0.1 mg_{Pt}/cm^2) as

basis.[1] Consequently, for the HEMFC systems, where we incorporated PdMo/C as the

ORR electrocatalyst, we assigned a value of 11.65 μm to t_{CCL}. This value would result

in a cost-wise equivalent cathode to 0.1 mg_{Pt}/cm^2 (the same cathode Pt loading as that

of the 2018 LDV PEMFC system). Similarly, for the PEMFC system, where we

incorporated Pt_3NiMo/C as the ORR electrocatalyst, we assigned a value of 13.84 μm

to t_{CCL}. This value would result in a cost-wise equivalent cathode to 0.1 mg_{Pt}/cm^2 (the

same cathode Pt loading as that of the 2018 LDV PEMFC system). For the HEMFC

system, where we incorporated Fe-N-C as the ORR electrocatalyst, we assigned a value

of 66.75 μm to t_{CCL}, which is the average of lower and higher bounds of t_{CCL}.

1.3 We set t_{ACL} for the FC systems that incorporated PM-containing HOR electrocatalysts

using the anode Pt loading of the 2018 LDV PEMFC system (0.025 mg_{Pt}/cm^2) as a

basis while making some adjustments based on the volumetric activity of the HOR

electrocatalysts.[1] Consequently, for the HEMFC systems, where we incorporated PM-

containing Ru_7Ni_3/C and PtRu/C as the HOR electrocatalysts, we assigned values of

29.71 μm and 1.72 μm to t_{ACL} of Ru_7Ni_3/C and PtRu/C. These values would result in

a cost-wise equivalent anode to 0.05 mg_{Pt}/cm^2, which is two times the Pt loading of the

2018 LDV PEMFC system. We chose the factor of two times to roughly compensate

for the lower HOR volumetric activity of Ru_7Ni_3/C and PtRu/C in alkaline electrolyte compared to the HOR volumetric activity of Pt/C in acidic electrolyte. For the PEMFC system, where we incorporated Pt/C as the HOR electrocatalyst, we assigned a value of 3.41 μm to t_{ACL}. This value would result in a cost-wise equivalent anode to 0.025 mg_{Pt}/cm^2 (the same anode Pt loading as the 2018 LDV PEMFC system). For the HEMFC systems, where we incorporated Ni/N-doped C as the HOR electrocatalyst, we assigned a value of 30.5 μm to t_{ACL}, which is the average of lower and higher bounds of t_{ACL}.

2. We optimized the total FC system cost using a 1-D FC sandwich model that operated based on the average inlet and exit pressure and composition of the anode and cathode gas channels. To calculate the average compositions of the anode and cathode gas channels, we assumed the exit RH of the anode and cathode gas channels to be the same as those calculated in step 1. In the ESI, we included more details about how, in a computationally efficient manner, we implemented the 1-D FC sandwich model in our cost optimization approach.

3. In this step, we ran the pseudo-2-D FC model using the FC stack operating conditions that resulted from the cost optimization in step 2 and updated the total FC system cost to the cost resulting from the pseudo-2-D FC model.

Details of determining the material and system developments needed to achieve the cost target of 30 $/kW_Net

We determined the material and system developments needed to decrease the HEMFC system cost to $30/$kW_{Net}$ based on PdMo/C-Ru_7Ni_3/C and (Fe-N-C)-Ni/N-doped C ORR-HOR

electrocatalyst pairs. We note that achieving the cost target of 30 $/kW$_{Net}$ is quite challenging, and we had to achieve it through a well-thought and balanced approach. In our approach: 1) We assumed reasonable ambitious improvements in the intrinsic activity of the HOR electrocatalyst, the ionic conductivity/H$_2$O permeability/local-O$_2$ transport resistance of the HEI, and some other improvements in the HEMFC stack components, 2) We assumed reasonable ambitious improvements in the performance of some of the BOP components and assumed a reasonable cost reduction in the CEM unit cost consistent with the cost reduction in the CEM unit outlined in the SA report,[1] and then 3) We determined how much improvement in the intrinsic activity of the ORR electrocatalysts is needed to attain the cost target of 30 $/kW$_{Net}$. We will explain in detail our assumptions regarding achieving the 30 $/kW$_{Net}$ cost target later. In this section, we explain how we determined the required improvements in the intrinsic activity of the ORR electrocatalyst to achieve the 30 $/kW$_{Net}$ cost target.

Determining the required improvement in the intrinsic activity of the ORR electrocatalysts needs a multi-step guess and check approach, which requires optimizing the total FC system cost in each guess and check iteration step. The intrinsic activity of an ORR electrocatalyst refers to the ORR specific activity (A/m^2_{ECSA}$) measured at 0.9 V vs. reversible hydrogen electrode (RHE), 25 °C, and 1 atm partial pressure (see Figure S2).

1. The free variables of global optimization are the FC stack operating parameters. We must assign a range to these parameters to perform the global optimization.

1.1 P_{Inlet}^{Stack} range: We assigned a lower bound of 1.31 atm and a higher bound of 2.5 atm to P_{Inlet}^{Stack}.

1.2 t_{CCL} range: For the HEMFC system, where we incorporated PdMo/C as the ORR electrocatalyst, we assigned a lower bound of 1 μm and a higher bound of 9 μm to t_{CCL}. For the HEMFC system, where we incorporated Fe-N-C as the ORR electrocatalyst, we assigned a lower bound of 1 μm and a higher bound of 70 μm to t_{CCL}.

1.3 t_{ACL} range: For the HEMFC system, where we incorporated Ru$_7$Ni$_3$/C as the HOR electrocatalyst, we assigned a lower bound of 1 μm and a higher bound of 9 μm to t_{ACL}. For the HEMFC system, where we incorporated Ni/N-doped C as the HOR electrocatalyst, we assigned a lower bound of 1 μm and a higher bound of 60 μm to t_{ACL}.

1.4 V_{Cell} range: We assigned a lower bound of 0.64 V and a higher bound of 0.9 V to V_{Cell}.

2. We calculated a reasonable estimate for the exit RH of the anode and cathode gas channels using the pseudo-2-D FC model for a FC operating with reasonable operating parameters described below and an ORR intrinsic activity equal to the intrinsic ORR activity of the electrocatalyst used in the HEMFC.

2.1 We assigned the values of P_{Inlet}^{Stack} and V_{Cell} to be the same as the values of P_{Inlet}^{Stack} and V_{Cell} of the 2018 LDV PEMFC system ($P_{Inlet}^{Stack} = 2.5\ atm$ and V_{Cell} $= 0.657\ atm$).[1]

2.2 For the HEMFC system, where we incorporated PdMo/C as the ORR electrocatalyst, we assigned a value of 5 μm to t_{CCL}, which is the average of lower and higher bounds of t_{CCL}. For the HEMFC system, where we incorporated Fe-N-C as the ORR

electrocatalyst, we assigned a value of 35.5 μm to t_{CCL}, which is the average of lower and higher bounds of t_{CCL}.

2.3 For the HEMFC system, where we incorporated Ru_7Ni_3/C as the HOR electrocatalyst, we assigned a value of 5 μm to t_{ACL}, which is the average of lower and higher bounds of t_{ACL}. For the HEMFC systems, where we incorporated Ni/N-doped C as the HOR electrocatalyst, we assigned a value of 30.5 μm to t_{ACL}, which is the average of lower and higher bounds of t_{ACL}.

3. We guessed a value for the intrinsic activity of the ORR electrocatalyst used in the HEMFC.

4. We optimized the total FC system cost using a 1-D FC sandwich model that operated based on the average inlet and exit pressure and composition of the anode and cathode gas channels. To calculate the average compositions of the anode and cathode gas channels, we assumed the exit RH of the anode and cathode gas channels to be the same as those calculated in step 2.

5. We calculated the total FC system cost using the 1-D FC sandwich model. If the total FC system cost was not 30 $/kW_{Net}$, we repeated 3 and 4.

6. In this step, we kept the FC stack operating conditions constant at values calculated in step 5. Then using the pseudo-2-D FC model, we made the required adjustments to the intrinsic activity of the ORR electrocatalyst calculated in step 5 until we achieved the cost target of 30 $/kW_{Net}$ based on the pseudo-2-D FC model.

Results and discussion

Determining the total HEMFC system cost based on currently available ORR and HOR electrocatalysts and comparison of the system cost of PEMFC and HEMFC

Determining the total HEMFC system cost based on currently available ORR and HOR electrocatalysts

We first sought to carefully compare and contrast the performance of state-of-the-art PM-containing and PM-free ORR and HOR electrocatalysts and then: 1) Choose the best electrocatalysts, irrespective of the electrocatalysts being PM-containing or PM-free, for implementation in our HEMFC system model, and 2) Choose the best PM-free electrocatalysts for implementation in our HEMFC system model due to the significant research interest in HEMFC community to develop entirely PM-free HEMFC systems.[6] We acknowledge the significant progress made thus far in developing unsupported electrocatalysts, but here we decided to limit our analysis to carbon-supported electrocatalysts. We made this informed decision for a couple of reasons. First, using high surface area carbon as support offers significant advantages: 1) Directly anchoring the ORR and HOR electrocatalysts to carbon support generally improves both performance and stability of the electrocatalysts within a FC.[36, 37] The performance improves because carbon support with high electrical conductivity ensures a low-resistance electron conducting pathway exists within the FC electrodes and provides ample porosity within the FC electrodes for H_2, O_2, and H_2O transport.[36, 37] The durability improves because carbon support confines/binds with the electrocatalyst particles, which reduces the likelihood of dissolution and physical delamination of the electrocatalysts,[36, 37] and 2) The electronic interactions between an electrocatalyst and carbon support can be easily tuned

by doping the carbon support, which can considerably boost the intrinsic activity of the electrocatalyst, which is a widely used approach to enhance the electrocatalytic activity of electrocatalysts.[10, 36] Second, the PEMFC LDV systems presented in the SA report (2018, 2020, and 2025) all are based on carbon-supported ORR and HOR electrocatalysts.[1] Third, to the best of our knowledge, all on-road FC LDVs today work based on carbon-supported ORR and HOR electrocatalysts.[1]

We compared and contrasted the performance of state-of-the-art PM-containing and PM-free ORR and HOR electrocatalysts using two critical metrics, namely the volumetric activity ($A/m^3_{Electrode}$) and the cost-based activity ($A/\$$) (Figure 3). An electrocatalyst with higher volumetric activity and cost-based activity would be a better choice for implementation in a FC system than an electrocatalyst with lower volumetric activity and cost-based activity. According to our literature review, each state-of-the-art PM-containing or PM-free electrocatalyst depicted in Figure 3 represents the highest volumetric and cost-based activity among electrocatalysts with similar components. For example, PdMo/C is the state-of-the-art Pd-based ORR electrocatalyst, which means that it has superior volumetric and cost-based activity compared to all Pd-based ORR electrocatalysts developed thus far. By close inspection of Figure 3, we can make three key observations. First, the PM-containing PdMo/C has the highest volumetric activity and cost-based activity among all ORR electrocatalysts and therefore is the best ORR electrocatalyst for implementation in a HEMFC system (Figure 3a). Second, the PM-free Fe-N-C has the highest volumetric activity and cost-based activity among all PM-free ORR electrocatalysts and therefore is the best PM-free ORR electrocatalyst for

implementation in an entirely PM-free HEMFC system (Figure 3a). Third, based on

volumetric and cost-based activity metrics, it is unclear which HOR electrocatalyst

(PtRu/C, Ru_7Ni_3/C, or Ni/N-doped C) is the best HOR electrocatalyst in alkaline

electrolyte (Figure 3b). Consequently, we examined all three HOR electrocatalysts in

HEMFC systems, where we incorporated PdMo/C as the ORR electrocatalyst. Ni/N-doped

C is the best PM-free HOR electrocatalyst, and consequently, we made our entirely PM-

free HEMFC system based on (Fe-N-C)-Ni/N-doped C ORR-HOR electrocatalyst pair.

Next, we calculated the total HEMFC system cost for the ORR-HOR electrocatalyst

pairs we chose above. Figure 4 compares the HEMFC system cost for the ORR-HOR

electrocatalyst pairs. Table 1 summarizes the HEMFC stack operating parameters,

geometric current density associated with a single cell in the HEMFC stack, and the

cathode outlet RH for the key pairs that we studied in this paper (we included similar

information for PdMo/C-PtRu/C and PdMo/C-Ni/N-doped C pairs in the ESI; Table S6).

We can make two critical conclusions by closely examining Figure 4. First, the HEMFC

system-level cost analysis shows that PdMo/C-Ru_7Ni_3/C is the cheapest HEMFC system,

and therefore Ru_7Ni_3/C is the best HOR electrocatalyst for implementation in a HEMFC

system. Second, as expected, the

(Fe-N-C)-Ni/N-doped C HEMFC system has the highest system cost among all

systems studied. We performed a detailed stack and BOP cost and voltage-loss breakdown

for PdMo/C-Ru_7Ni_3/C and (Fe-N-C)-Ni/N-doped C HEMFC systems, allowing us to

identify the highest cost and voltage-loss drivers in HEMFC systems (Figure 5). We can

extract three key results from a close inspection of Figure 5. First, for the PdMo/C-

Ru$_7$Ni$_3$/C HEMFC system, the four highest cost drivers of the stack are C$_{Balance\ of\ stack}$ >

C$_{Bipolar\ plate}$ > C$_{Cathode\ electrocatalyst}$ > C$_{GDL}$ ≈ C$_{Subgasket}$, where C is the cost (Figure 5a). For the

(Fe-N-C)-Ni/N-doped C HEMFC system, the four highest cost drivers of the stack are

C$_{Bipolar\ plate}$ > C$_{Balance\ of\ stack}$ > C$_{GDL}$ ≈ C$_{Subgasket}$ (Figure 5b). Second, for the PdMo/C-

Ru$_7$Ni$_3$/C HEMFC system, the four highest cost drivers of the BOP are C$_{Air\ management\ system}$

>> C$_{Additional\ balance\ of\ plant}$ > C$_{Thermal\ management\ system}$ > C$_{Humidification\ management\ system}$ (Figure 5c).

For the (Fe-N-C)-Ni/N-doped C HEMFC system, the four highest cost drivers of the BOP

are C$_{Air\ management\ system}$ >> C$_{Additional\ balance\ of\ plant}$ > C$_{Thermal\ management\ system}$ > C$_{Fuel\ management\ system}$

(Figure 5d). Third, for the PdMo/C-Ru$_7$Ni$_3$/C HEMFC system, the four highest voltage-

loss drivers are $\Delta V_{Cathode\ kinetic}$ >> $\Delta V_{Anode\ kinetic}$ > $\Delta V_{Concentration}$ > $\Delta V_{Electronic}$, where ΔV is

the voltage-loss (Figure 5e). For the (Fe-N-C)-Ni/N-doped C HEMFC system, the four

highest voltage-loss drivers are $\Delta V_{Cathode\ kinetic}$ >> $\Delta V_{Anode\ kinetic}$ > $\Delta V_{Cathode\ ionic}$ > ΔV_{Anode}

$_{ionic}$ ≈ $\Delta V_{Concentration}$ (Figure 5f). We note that $\Delta V_{Cathode\ ionic}$ and $\Delta V_{Anode\ ionic}$ play a more

prominent role in creating voltage loss in (Fe-N-C)-Ni/N-doped C HEMFC system

because of the much thicker cathode and anode electrodes in this system (Table 1).

Developing PM-free ORR and HOR electrocatalysts has recently attracted significant

interest in the HEMFC community on the proposed premise that removing PMs from the

cathode and anode electrodes will considerably reduce the HEMFC stack cost.[6] However,

this premise does not account for the significantly superior intrinsic activity of the state-

of-the-art PM-containing ORR and HOR electrocatalysts compared to PM-free ORR and

HOR electrocatalysts. The superior intrinsic activity of the PM-containing ORR and HOR

electrocatalysts enables considerably higher stack power density for PM-based HEMFC

stacks than PM-free HEMFC stacks. Consequently, PM-based HEMFC stacks will have substantially smaller stack areas than PM-free stacks, resulting in PM-based HEMFC stacks being considerably cheaper than PM-free HEMFC stacks. One can clearly see this concept by comparing the HEMFC stack area and cost of $PdMo/C-Ru_7Ni_3/C$ and (Fe-N-C)-Ni/N-doped C HEMFC systems (Figure 5a and 5b). We finish this section by noting that the total stack area of the 2018 LDV PEMFC system described in the SA report is 7.486 m^2,[1] so we can see that while the stack area of $PdMo/C-Ru_7Ni_3/C$ HEMFC system is very reasonable, the stack area of the (Fe-N-C)-Ni/N-doped C HEMFC system is prohibitively large for practical FC-based LDVs.

Comparison of the system cost of PEMFC and HEMFC

In this section, we sought to compare the system cost of PEMFC and HEMFC fairly. We decided to make this comparison as it is not known a priori that a HEMFC system should be cheaper than a PEMFC system. As explained in detail in the introduction, there are reasonable arguments for the HEMFC system having a cheaper stack than the PEMFC system. However, the HEMFC system faces two significant hurdles that would increase its system cost compared to the PEMFC system. First, as explained in detail in the introduction, due to the technologically intolerable atmospheric CO_2-induced voltage losses, HEMFC systems must incorporate CO_2 scrubbing of air before the air enters the HEMFC stack. Incorporating an EDCS unit in the HEMFC system appears to be the most sensible approach currently available for CO_2 removal from the atmospheric air, which will increase the HEMFC system's cost compared to the PEMFC system. Second, as explained in detail in the ESI, the H_2O generation, consumption, and movement resulting

from electro-osmotic drag in PEMFC and HEMFC are markedly different.[22, 37, 38] In PEMFC, H_2O is an ORR product generated only in the cathode, and no H_2O is generated/consumed in the HOR in the anode.[37, 38] Also, protons drag H_2O molecules with themselves as they go from the anode to the cathode side of the PEMFC.[37, 39] In contrast, in HEMFC, H_2O serves as a reactant in the ORR in the cathode and as a product in the HOR in the anode.[22] Furthermore, hydroxides drag H_2O molecules with themselves as they go from the cathode to the anode side of the HEMFC.[22] Because of this markedly different H_2O behavior in PEMFC and HEMFC, we expect the cathode outlet RH of HEMFC to be lower than that of PEMFC, resulting in a more expensive humidification management system cost for the HEMFC, which will increase the HEMFC system's cost compared to the PEMFC system.

We note that neglecting PdMo/C, the PM-containing Pt_3NiMo/C has the highest volumetric and cost-based activity among all ORR electrocatalysts, and we chose Pt_3NiMo/C as the ORR electrocatalyst for the PEMFC system (Figure 3). We made this choice as PdMo/C is an ORR electrocatalyst specifically designed for alkaline electrolyte, and in acidic electrolyte, it has very poor stability that is insufficient for practical applications.[11] We chose Pt/C as the HOR electrocatalyst for the PEMFC system for two reasons: 1) The HOR kinetics of Pt/C in acidic electrolyte is very facile, and the HOR activity of Pt/C is considered to be adequate for PEMFC LDVs, and the focus of PEMFC community is on developing more active ORR electrocatalysts,[27, 37, 40] and 2) The PEMFC LDV systems presented in the SA report (2018, 2020, and 2025) all are based on Pt/C HOR electrocatalyst.[1] Interestingly, Figure 3 shows that the HOR volumetric activity and

cost-based activity of Pt/C in acidic electrolyte is higher than all the state-of-the-art carbon-supported PM-containing and PM-free HOR electrocatalysts in alkaline electrolyte.

Table 1 summarizes the stack operating parameters, geometric current density associated with a single cell in the stack, and the cathode outlet RH for the Pt_3NiMo/C-Pt/C PEMFC system. We included the cost of the Pt_3NiMo/C-Pt/C PEMFC system in Figure 4. Figure 4 shows that the cost of the Pt_3NiMo/C-Pt/C PEMFC system is lower than the $PdMo/C$-Ru_7Ni_3/C HEMFC system. To examine the underlying reason for our observation and to provide more insights into the differences between PEMFC and HEMFC systems, we performed a detailed stack and BOP cost and voltage-loss breakdown for the Pt_3NiMo/C-Pt/C PEMFC system, and we compared the results with that of the $PdMo/C$-Ru_7Ni_3/C HEMFC system in Figure 6. We can extract three key results from a close inspection of Figure 6. First, for the Pt_3NiMo/C-Pt/C PEMFC system, the four highest cost drivers of the stack are $C_{Bipolar\ plate} > C_{Balance\ of\ stack} > C_{Cathode\ electrocatalyst} > C_{GDL} \approx C_{Subgasket}$ (Figure 6a). We can see that the $PdMo/C$-Ru_7Ni_3/C HEMFC system has a cheaper stack (1.93 $/kW$_{Net}$) compared with the Pt_3NiMo/C-Pt/C PEMFC system (Figure 6a and 6b). Second, for the Pt_3NiMo/C-Pt/C PEMFC system, the four highest cost drivers of the BOP are $C_{Air\ management\ system} \gg C_{Additional\ balance\ of\ plant} > C_{Thermal\ management\ system} > C_{Fuel\ management\ system}$ (Figure 6c). The $PdMo/C$-Ru_7Ni_3/C HEMFC system has a more expensive BOP compared with the Pt_3NiMo/C-Pt/C PEMFC system (4.59 $/kW$_{Net}$), which is caused mainly by EDCS cost (2.04 $/kW$_{Net}$) and humidification management system extra cost (1.68 $/kW$_{Net}$) (Figure 6c and 6d). The higher cost of the humidification management system for the $PdMo/C$-Ru_7Ni_3/C HEMFC system is caused by the fact that,

as we expected, the PdMo/C-Ru$_7$Ni$_3$/C HEMFC system operates at a lower cathode outlet RH compared to the Pt$_3$NiMo/C-Pt/C PEMFC system (Table 1). Overall, the cost increases in the BOP of the PdMo/C-Ru$_7$Ni$_3$/C HEMFC system are higher than the cost savings in its stack when compared with the Pt$_3$NiMo/C-Pt/C PEMFC system, which results in the PdMo/C-Ru$_7$Ni$_3$/C HEMFC system having a higher cost than the Pt$_3$NiMo/C-Pt/C PEMFC system by 2.65 \$/kW$_{Net}$. Third, for the Pt$_3$NiMo/C-Pt/C PEMFC system, the four highest voltage-loss drivers are $\Delta V_{Cathode\ kinetic} \gg \Delta V_{Electronic} > \Delta V_{Concentration} > \Delta V_{Cathode\ ionic}$ (Figure 6e). We note that while $\Delta V_{Anode\ kinetic}$ is the second biggest voltage-loss driver in the PdMo/C-Ru$_7$Ni$_3$/C HEMFC system, it is not even among the four highest voltage-loss drivers in the Pt$_3$NiMo/C-Pt/C PEMFC system (Figure 6e and 6f). This observation means that more research and development efforts are required to improve the activity of the HOR electrocatalysts in alkaline electrolyte.

We want to finish this section by mentioning that the goal of the comparison of the PEMFC system and HEMFC system in this section was not to encourage the use of one of these FC technologies over the other. Our goal was to identify and analyze each system's major cost and voltage drivers. This analysis will enable future research and development efforts to focus on these major cost and voltage loss drivers to achieve the greatest benefit for commercialization purposes. Which one of these FC technologies would be the preferable choice for LDV applications will ultimately depend on which one of these technologies can reach the ultimate cost target of 30 \$/kW$_{Net}$, and at the same time, meet or exceed the stringent durability requirements set by DOE for LDV applications.[6, 41]

Determining the material and system developments needed to decrease the HEMFC system

cost to 30 $/kW_{Net} and investigating the relative importance of operating parameters of the

EDCS unit through single variable sensitivity analysis

Determining the material and system developments needed to decrease the HEMFC system

cost to 30 $/kW_{Net}

In this section, we sought to determine the material and system developments needed

to decrease the HEMFC system cost to 30 $/kW$_{Net}$ based on PdMo/C-Ru$_7$Ni$_3$/C) and (Fe-

N-C)-Ni/N-doped C ORR-HOR electrocatalyst pairs. As mentioned before, achieving the

cost target of 30 $/kW$_{Net}$ is quite challenging, and we had to achieve it through a well-

thought and balanced three-step approach. In the first step of our approach, we assumed

reasonably ambitious improvements in the intrinsic activity of the HOR electrocatalyst

(i.e., exchange current density measured at 25 °C and 1 atm partial pressure (see Figure

S2); A/m^2$_{ECSA}$), the ionic conductivity/H$_2$O permeability/local-O$_2$ transport resistance of

the HEI, and some other improvements in the HEMFC stack components. We also

assumed that these improvements in the performance of the components of the HEMFC

stack, which should be realized through engineering and scientific research and

innovation, would not change the cost of the components. We summarized our

assumptions here; Interested readers can find more details about them in the ESI.

1) The HOR intrinsic activity of Pt/C in acidic electrolyte is higher than all the state-

of-the-art carbon-supported PM-containing and PM-free HOR electrocatalysts in

alkaline electrolyte (Figure S2b). The literature results attribute this observation

either to unfavorable H$_2$O hydrogen bonding structure over the electrocatalyst

surface or unfavorable H_2O-surface binding energy in alkaline electrolyte.[42-45] Finetuning the H_2O hydrogen bonding structure and/or H_2O-surface binding energy and reverting it entirely to its state in acidic electrolyte will be an arduous task. Consequently, we assumed that the intrinsic activity of the Ru_7Ni_3/C and Ni/N-doped C HOR electrocatalyst could be increased by fifteen times (Figure S2b).

2) We assumed the HEI's ionic conductivity and H_2O permeability could be increased to three times that of 700 g/mol EW PEI and that local-O_2 transport resistance of the HEI could be decreased from 25 s/cm to 6 s/cm.

3) We assumed that the thickness of the GDL and MPL could be reduced from the values specified in the SA report (105 μm and 45 μm)[1] to (90 μm and 20 μm).

4) We assumed the total area-specific electronic resistance could be reduced from 20 mΩ.cm^2 to 10 mΩ.cm^2.

In the second step, we assumed reasonable ambitious improvements in the performance of some of the BOP components. We also assumed that these improvements in the performance of the BOP components, which should be realized through engineering and scientific research and innovation, would not change the cost of the components. We also adopted a reasonable cost reduction in the CEM unit cost consistent with the cost reduction in the CEM unit outlined in the SA report. We summarized our assumptions here; Interested readers can find more details about them in the ESI.

1) As detailed in ESI, the membrane humidifier has a composite four-layer membrane which consists of a 180 μm polyethylene terephthalate (PET) porous layer, a 10 μm ePTFE layer, a 5 μm layer of H_2O transport membrane, and another 10 μm ePTFE layer. We assumed that the thickness of the PET layer and two ePTFE layers could be reduced to 85 μm and 7 μm. We also assumed that the H_2O permeability of the H_2O transport membrane could be increased by two and a half times.

2) We assumed that the pressure drop of the EDCS unit ($\Delta P_{EDCS} = 0.072\ atm$) and total CO_2 capture mass transport resistance of EDCS unit ($R_{MT} = 10\left(\frac{s}{m}\right) + 4\left(\frac{s}{m.\,atm}\right)P_{EDCS}$) could be reduced by 50 % ($\Delta P_{EDCS} = 0.036\ atm\ and\ R_{MT} = 5\left(\frac{s}{m}\right) + 2\left(\frac{s}{m.\,atm}\right)P_{EDCS}$).

3) Consistent with the cost reduction in the CEM unit cost outlined in the SA report, we applied a cost correction term to the air management system cost model (see the ESI for detailed discussion).

In the third step, we determined how much improvement in the intrinsic activity of the ORR electrocatalysts (i.e., the ORR specific activity (A/m^2_{ECSA}) measured at 0.9 V vs. RHE, 25 °C and 1 atm partial pressure; Figure S2a) is needed to attain the cost target of 30 $/kW_{Net}$. We found that achieving the cost target of 30 $/kW_{Net}$ requires the ORR intrinsic activity of PdMo/C and Fe-N-C electrocatalysts to be increased by 17.07 and 664.91 times. Table 1 summarizes the HEMFC stack operating parameters, geometric current density associated with a single cell in the HEMFC stack, and the cathode outlet RH for 30 $/kW_{Net}$ PdMo/C-Ru$_7$Ni$_3$/C and (Fe-N-C)-Ni/N-doped C HEMFC systems. The

arrows in Figure 3 demonstrate how much improvements in the volumetric and cost-based activities of the ORR and HOR electrocatalysts are required to achieve the cost target of 30 $/kW$_{Net}$ for PdMo/C-Ru$_7$Ni$_3$/C and (Fe-N-C)-Ni/N-doped C HEMFC systems. By closely examining Figure 3, we can see that the easiest path to achieve the cost target of 30 $/kW$_{Net}$ is to develop PM-based ORR and HOR electrocatalysts. Of particular note, to achieve the cost target of 30 $/kW$_{Net}$, the volumetric activity of Fe-N-C electrocatalyst needs to significantly improve beyond that of Pt/C electrocatalyst and even go beyond that of PdMo/C electrocatalyst, which probably will be a tall order (Figure 3a).

We performed a detailed stack and BOP cost and voltage-loss breakdown for 30 $/kW$_{Net}$ PdMo/C-Ru$_7$Ni$_3$/C and (Fe-N-C)-Ni/N-doped C HEMFC systems, allowing us to identify the highest cost and voltage-loss drivers in these HEMFC systems (Figure 7). We can extract three key results from the close inspection of Figure 7. First, for the 30 $/kW$_{Net}$ PdMo/C-Ru$_7$Ni$_3$/C HEMFC system, the four highest cost drivers of the stack are $C_{\text{Balance of stack}} > C_{\text{Bipolar plate}} > C_{\text{Cathode electrocatalyst}} > C_{\text{GDL}} \approx C_{\text{Subgasket}}$ (Figure 7a). For the 30 $/kW$_{Net}$ (Fe-N-C)-Ni/N-doped C HEMF system, the four highest cost drivers of the stack are $C_{\text{Balance of stack}} > C_{\text{Bipolar plate}} > C_{\text{GDL}} \approx C_{\text{Subgasket}}$ (Figure 7b). Second, for the 30 $/kW$_{Net}$ PdMo/C-Ru$_7$Ni$_3$/C HEMFC system, the four highest cost drivers of the BOP are $C_{\text{Air management system}} > C_{\text{Additional balance of plant}} > C_{\text{Thermal management system}} > C_{\text{Fuel management system}}$ (Figure 7c). For the 30 $/kW$_{Net}$ (Fe-N-C)-Ni/N-doped C HEMFC system, the four highest cost drivers of the BOP are $C_{\text{Air management system}} > C_{\text{Additional balance of plant}} > C_{\text{Thermal management system}} > C_{\text{Fuel management system}}$ (Figure 7d). We also want to highlight the fact that both the 30 $/kW$_{Net}$ PdMo/C-Ru$_7$Ni$_3$/C HEMFC system and the 30 $/kW$_{Net}$ (Fe-N-C)-Ni/N-doped C HEMFC

system operate at P_{Inlet}^{Stack} of 1.31 atm; therefore, they correspond to FC systems that do not need an expander (i.e., the air stream enters the expander at atmospheric pressure; Table 1). Third, for the 30 \$/kW$_{Net}$ PdMo/C-Ru$_7$Ni$_3$/C HEMFC system, the four highest voltage-loss drivers are $\Delta V_{Cathode\ kinetic} \gg \Delta V_{Concentration} > \Delta V_{Electronic} > \Delta V_{Anode\ kinetic}$ (Figure 7e). For the 30 \$/kW$_{Net}$ (Fe-N-C)-Ni/N-doped C HEMFC system, the four highest voltage-loss drivers are $\Delta V_{Cathode\ kinetic} \gg \Delta V_{Concentration} > \Delta V_{Cathode\ ionic} > \Delta V_{Electronic}$ (Figure 7f).

Investigating the relative importance of operating parameters of the EDCS unit through single variable sensitivity analysis

The EDCS unit can affect the HEMFC system cost not only through the required cost to make the EDCS unit but also through the H$_2$ consumed to CO$_2$ removed ratio and pressure drop of the EDCS unit (ΔP_{EDCS}). This fact motivated us to investigate and elucidate the relative importance of the EDCS unit cost, the H$_2$ consumed to CO$_2$ removed ratio, and ΔP_{EDCS} through single variable sensitivity analysis. We performed our single variable sensitivity analysis on two HEMFC systems: 1) The base-case PdMo/C-Ru$_7$Ni$_3$/C HEMFC system and 2) The 30 \$/kW$_{Net}$ PdMo/C-Ru$_7$Ni$_3$/C HEMFC system. In our single variable sensitivity analysis, we kept the HEMFC stack operating parameters constant, reduced the value of the parameter of interest by one percent, and then calculated how much the HEMFC system cost changed on a normalized scale. We highlight two crucial points before discussing the single variable sensitivity analysis results. First, as we discussed in the ESI, we defined a parameter named f_{O_2}, which is the ratio of the molar flow rate of O$_2$ consumed in the EDCS unit to the molar flow rate of O$_2$ entering the stack. In the ESI, we showed that f_{O_2} is linearly proportional to the H$_2$ consumed to CO$_2$ removed

ratio in the EDCS unit.   (i.e., a one percent reduction in f_{O_2} results in a one percent reduction in the H_2 consumed to CO_2 removed ratio). Second, as we discussed in the ESI, the EDCS unit cost (C_{EDCS}; $) can be calculated using equation 2.

$$C_{EDCS} = A_{EDCS} \times Cost_{EDCS-Area\,based}; \ A_{EDCS} = R_{MT}\dot{V}_{EDCS} \times \ln\left(\frac{x_{CO_2}^{Inlet\,EDCS}}{x_{CO_2}^{Outlet\,EDCS}}\right) (2)$$

In equation 2, (A_{EDCS}; m²), ($Cost_{EDCS-Area\,based}$; \$/m²), ($x_{CO_2}^{Inlet\,EDCS} = 420\,ppm$), ($x_{CO_2}^{Outlet\,EDCS} = 4\,ppm$), ($\dot{V}_{EDCS}$; m³/s), and ($R_{MT}$; s/m) are the required EDCS active area, the area-based cost of the EDCS, the mole fraction of CO_2 in the EDCS inlet air stream, the mole fraction of CO_2 in the EDCS outlet air stream, the volumetric flow rate of air at the conditions within the EDCS and the total CO_2 capture mass transport resistance. We can see from equation 2 that C_{EDCS} is linearly proportional to $Cost_{EDCS-Area\,based}$ and R_{MT}. Therefore, we can perform the single variable sensitivity analysis of C_{EDCS} by changing either the parameter $Cost_{EDCS-Area\,based}$ or R_{MT} (i.e., a one percent reduction in either $Cost_{EDCS-Area\,based}$ or R_{MT} results in a one percent reduction in C_{EDCS}).

Considering the logic presented in the above two points, we performed the single variable sensitivity analysis by changing the parameters f_{O_2}, ΔP_{EDCS}, and $Cost_{EDCS-Area\,based}$, and subsequently, we presented the results in Figure 8. By closely inspecting Figure 8, we can make three critical observations. First, there is no need to reduce f_{O_2} (or equivalently, the H_2 consumed to CO_2 removed ratio), since, as we can see from Figure 8, reducing f_{O_2} increases the HEMFC system cost. This cost increase is entirely caused by the fact that reducing f_{O_2} increases the humidification management system cost because it reduces the gaseous H_2O that ends up in the airflow of the EDCS,

and therefore it increases the humidification requirement and the cost of the membrane humidifier (equation S114 in the ESI). Second, our analysis demonstrates that reducing ΔP_{EDCS} reduces the overall HEMFC system cost, and its effect on a normalized scale on the 30 $/kW$_{\text{Net}}$ PdMo/C-Ru$_7$Ni$_3$/C HEMFC system is more pronounced than its effect on the base-case PdMo/C-Ru$_7$Ni$_3$/C HEMFC system. Third, our analysis demonstrates that reducing $Cost_{EDCS-Area\,based}$ reduces the overall HEMFC system cost, but its effect on a normalized scale on the 30 $/kW$_{\text{Net}}$ PdMo/C-Ru$_7$Ni$_3$/C HEMFC system is less pronounced than its effect on the base-case (PdMo/C-Ru$_7$Ni$_3$/C) HEMFC system.

We want to finish this section by mentioning that measuring the value of (ΔP_{EDCS}) and establishing the strategies to control/reduce it for EDCS units processing technologically relevant air flow rates corresponding to an 80 kW$_{\text{Net}}$ HEMFC stack should be a fundamental and urgent future research goal for the HEMFC community for two reasons. First, as we can observe in Figure 8, ΔP_{EDCS} significantly impacts the overall HEMFC system cost, comparable to the $Cost_{EDCS-Area\,based}$. Second, the EDCS research and development efforts up until now have been solely focused on reducing R_{MT}.[25, 26] While this is a conceptually sound research strategy, the improvements in R_{MT} have been achieved by using air flow mediums with high inherent pressure drops that are not typically used in the FC industry, namely interdigitated flow fields and polypropylene/nickel mesh.[25, 26] Interdigitated flow fields are the flow fields of choice for redox flow batteries.[46] The flow field structure forces fluid flow into a portion of the electrode, which improves mass transport at the cost of increased pressure drop.[46] As a point of comparison, United Technologies' benchmark computational fluid dynamic (CFD) results demonstrate that at

equal area-specific flow rates and channel lengths, typical interdigitated flow fields have about four times higher pressure drops than parallel flow fields.[46] Polypropylene and nickel mesh are porous mediums that will exert significant skin friction on the fluid flow through them. As a point of comparison, United Technologies' benchmark CFD results demonstrate that at equal area-specific flow rates and channel lengths, fluid flow through fibrous porous mediums with permeabilities of 10^{-10} m^2 and 10^{-9} m^2 will create pressure drops of about 50 to 5 times higher than the pressure drop of parallel flow fields.[46] The high inherent pressure drop of these air flow mediums clearly signifies the need to measure and control the pressure drop in EDCS units that are built based on them and process technologically relevant air flow rates.

Conclusions

Our study demonstrates that the most promising approach to achieve the cost target of 30 \$/kW$_{Net}$ is developing PM-containing ORR and HOR electrocatalysts that enable higher power density HEMFC stacks. Our comparison between HEMFC and PEMFC systems showed that the HEMFC system has a cheaper stack but a more expensive BOP than the PEMFC system, resulting in a higher HEMFC system cost. The higher HEMFC system cost is due to EDCS cost and higher humidification management system cost caused by the lower cathode outlet relative humidity of HEMFC compared with that of PEMFC. In addition, our single variable sensitivity analysis indicated that EDCS pressure drop significantly impacts the overall HEMFC system cost, comparable to the area-based cost and that one must monitor its values in future studies. Finally, we identified the cost and voltage-loss drivers for all systems studied in this paper. Overall, our work provides

valuable directions for the strategic development of HEMFC system components by identifying the highest cost and voltage-loss drivers in HEMFC systems and analyzing the relative importance of EDCS operating parameters.

We finish this paper by noting that two essential metrics should be realized in tandem to enable affordable FC-based cars for the mass market. One is the FC light-duty vehicle (LDV) cost which is the subject of our paper, and the other metric is adequate durability for the components of the FC-based LDV system. The Hydrogen and Fuel Cell Technologies Office of DOE has already set the required durability targets for the components of the FC-based LDV systems for commercialization[41] (these requirements have been set for PEMFC-based LDVs, but they will similarly be required for HEMFC-based LDVs).[6] The materials and development needs described in our paper should be satisfied in tandem with the durability requirements set by the Hydrogen and Fuel Cell Technologies Office of DOE to make the goal of affordable and durable HEMFC cars a reality.

Author contributions section

Dr. Reza Abbasi conceived the ideas and was engaged in data analysis. He performed the technoeconomic analysis and acquired all the data. He was a significant contributor to the initial outline of the paper, and he wrote the initial draft of the paper and revised it according to the feedback from the other co-authors. Dr. Brian P. Setzler conceived the ideas and was engaged in data analysis. He was a significant contributor to the initial outline of the paper, and he read the initial draft of the paper and provided feedback for revisions. Prof. Yushan Yan conceived the ideas and was engaged in data analysis. He was a significant contributor to the initial outline of the paper, and he read the initial draft of the paper and provided feedback for revisions.

Conflicts of interest

Yushan Yan is the founder and CEO of Versogen, Inc., a manufacturer of HEMs. Brian Setzler is a co-founder and employee of Versogen.

Acknowledgments

References

1.   B. D. James, J. M. Huya-Kouadio, C. Houchins and D. A. DeSantis, *Mass Production Cost Estimation of Direct H₂ PEM Fuel Cell Systems for Transportation Applications: 2018 Update*, 2018.

2.   S. T. Thompson, B. D. James, J. M. Huya-Kouadio, C. Houchins, D. A. DeSantis, R. Ahluwalia, A. R. Wilson, G. Kleen and D. Papageorgopoulos, *Journal of Power Sources*, 2018, **399**, 304-313.

3.   R. Abbasi, B. P. Setzler, S. Lin, J. Wang, Y. Zhao, H. Xu, B. Pivovar, B. Tian, X. Chen and G. Wu, *Advanced Materials*, 2019, **31**, 1805876.

4.   Toyota moves to expand mass-production of fuel cell stacks and hydrogen tanks towards ten-fold increase post-2020. Toyota Europe Newsroom, https://newsroom.toyota.eu/toyota-moves-to-expand-mass-production-of-fuel-cell-stacks-and-hydrogen-tanks-towards-ten-fold-increase-post-2020/, 2023).

5.   S. Kim, Hyundai plans $6.7 billion investment to boost fuel-cell output. Bloomberg, https://www.bloomberg.com/news/articles/2018-12-11/hyundai-plans-6-7-billion-investment-to-boost-fuel-cell-output?leadSource=uverify%20wall, 2023).

6.   S. T. Thompson, D. Peterson, D. Ho and D. Papageorgopoulos, *Journal of The Electrochemical Society*, 2020, **167**, 084514.

7.   H. Adabi, A. Shakouri, N. Ul Hassan, J. R. Varcoe, B. Zulevi, A. Serov, J. R. Regalbuto and W. E. Mustain, *Nature energy*, 2021, **6**, 834-843.

8.   Z. Xu, X. Zhang, X. Wang, J. Fang, Y. Zhang, X. Liu, W. Zhu, Y. Yan and Z.

Zhuang, *ACS nano*, 2021, **15**, 7131-7138.

9.   Y. Yang, H. Peng, Y. Xiong, Q. Li, J. Lu, L. Xiao, F. J. DiSalvo, L. Zhuang and H. c. D. Abruña, *ACS Energy Letters*, 2019, **4**, 1251-1257.

10.   W. Ni, T. Wang, F. Héroguel, A. Krammer, S. Lee, L. Yao, A. Schüler, J. S. Luterbacher, Y. Yan and X. Hu, *Nature Materials*, 2022, 1-7.

11.   M. Luo, Z. Zhao, Y. Zhang, Y. Sun, Y. Xing, F. Lv, Y. Yang, X. Zhang, S. Hwang and Y. Qin, *Nature*, 2019, **574**, 81-85.

12.   G. Huang, M. Mandal, X. Peng, A. C. Yang-Neyerlin, B. S. Pivovar, W. E. Mustain and P. A. Kohl, *Journal of The Electrochemical Society*, 2019, **166**, F637.

13.   N. Ul Hassan, M. Mandal, G. Huang, H. A. Firouzjaie, P. A. Kohl and W. E. Mustain, *Advanced Energy Materials*, 2020, **10**, 2001986.

14.   X. Peng, D. Kulkarni, Y. Huang, T. J. Omasta, B. Ng, Y. Zheng, L. Wang, J. M. LaManna, D. S. Hussey and J. R. Varcoe, *Nature communications*, 2020, **11**, 1-10.

15.   J. Wang, Y. Zhao, B. P. Setzler, S. Rojas-Carbonell, C. Ben Yehuda, A. Amel, M. Page, L. Wang, K. Hu and L. Shi, *Nature Energy*, 2019, **4**, 392-398.

16.   M. Mandal, G. Huang, N. U. Hassan, X. Peng, T. Gu, A. H. Brooks-Starks, B. Bahar, W. E. Mustain and P. A. Kohl, *Journal of The Electrochemical Society*, 2019, **167**, 054501.

17.   S. Gottesfeld, D. R. Dekel, M. Page, C. Bae, Y. Yan, P. Zelenay and Y. S. Kim, *Journal of Power Sources*, 2018, **375**, 170-184.

18.   D. R. Dekel, *Journal of Power Sources*, 2018, **375**, 158-169.

19.   W. E. Mustain, *Current Opinion in Electrochemistry*, 2018, **12**, 233-239.

20.   T. Wang, L. Shi, J. Wang, Y. Zhao, B. P. Setzler, S. Rojas-Carbonell and Y. Yan, *Journal of The Electrochemical Society*, 2019, **166**, F3305.

21.   W. E. Mustain, M. Chatenet, M. Page and Y. S. Kim, *Energy & Environmental Science*, 2020, **13**, 2805-2838.

22.   M. R. Gerhardt, L. M. Pant and A. Z. Weber, *Journal of The Electrochemical Society*, 2019, **166**, F3180.

23.   Y. Zheng, G. Huang, M. Mandal, J. R. Varcoe, P. A. Kohl and W. E. Mustain, *Journal of The Electrochemical Society*, 2021, **168**, 024504.

24.   Y. Zheng, T. J. Omasta, X. Peng, L. Wang, J. R. Varcoe, B. S. Pivovar and W. E. Mustain, *Energy & Environmental Science*, 2019, **12**, 2806-2819.

25.   S. Matz, B. P. Setzler, C. M. Weiss, L. Shi, S. Gottesfeld and Y. Yan, *Journal of The Electrochemical Society*, 2021, **168**, 014501.

26.   L. Shi, Y. Zhao, S. Matz, S. Gottesfeld, B. P. Setzler and Y. Yan, *Nature Energy*, 2022, **7**, 238-247.

27.   A. Kongkanand and M. F. Mathias, *The journal of physical chemistry letters*, 2016, **7**, 1127-1137.

28.   Bureau of Labor Statistics, Table of Producer Price Index (PPI) commodity data for finished goods series ID: WPUFD49207, https://data.bls.gov/cgi-bin/surveymost?wp, 2023).

29.   Johnson Matthey, PGM prices and trading, https://matthey.com/products-and-markets/pgms-and-circularity/pgm-management/, (accessed 2023).

30.   The London Metal Exchange, Metals prices, https://www.lme.com/en/Metals,

(accessed 2023).

31.   B. D. James, J. M. Huya-Kouadio, C. Houchins and D. A. DeSantis, *Mass Production Cost Estimation of Direct H$_2$ PEM Fuel Cell Systems for Transportation Applications: 2015 Update*, 2015.

32.   K.-F. Man, K. S. Tang and S. Kwong, *Genetic algorithms: concepts and designs*, Springer Science & Business Media, 2001.

33.   M. Mitchell, *An introduction to genetic algorithms* The MIT press, Cambridge, Massachusetts, London, England, 1996.

34.   C. M. Tan, *Simulated annealing*, BoD–Books on Demand, 2008.

35.   P. J. Van Laarhoven and E. H. Aarts, *Simulated annealing: Theory and Applications*, Springer, 1987.

36.   E. Antolini, *Applied Catalysis B: Environmental*, 2009, **88**, 1-24.

37.   W. Vielstich, A. Lamm and H. Gasteiger, *Handbook of fuel cells. Fundamentals, technology, applications*, Wiley, 2003.

38.   K. Neyerlin, W. Gu, J. Jorne and H. A. Gasteiger, *Journal of the Electrochemical Society*, 2006, **153**, A1955.

39.   T. A. Zawodzinski, J. Davey, J. Valerio and S. Gottesfeld, *Electrochimica Acta*, 1995, **40**, 297-302.

40.   K. Neyerlin, W. Gu, J. Jorne and H. A. Gasteiger, *Journal of The Electrochemical Society*, 2007, **154**, B631.

41.   U.S. Department of Energy Fuel Cell Technologies Office, "Fuel cells multi-year research, development & demonstration plan."

https://www.energy.gov/sites/prod/files/2017/05/f34/fcto_myrdd_fuel_cells.pdf,

2023).

42.   X. Yang, J. Nash, N. Oliveira, Y. Yan and B. Xu, *Angewandte Chemie*, 2019, **131**,

17882-17887.

43.   T. Cheng, L. Wang, B. V. Merinov and W. A. Goddard III, *Journal of the American

Chemical Society*, 2018, **140**, 7787-7790.

44.   J. Zheng, J. Nash, B. Xu and Y. Yan, *Journal of The Electrochemical Society*, 2018,

165, H27.

45.   Y. Xue, L. Shi, X. Liu, J. Fang, X. Wang, B. P. Setzler, W. Zhu, Y. Yan and Z.

Zhuang, *Nature communications*, 2020, **11**, 1-8.

46.   M. MacDonald and R. M. Darling, *AIChE Journal*, 2018, **64**, 3746-3755.

47.   X. Huang, Z. Zhao, L. Cao, Y. Chen, E. Zhu, Z. Lin, M. Li, A. Yan, A. Zettl and Y.

M. Wang, *Science*, 2015, **348**, 1230-1234.

48.   W. Sheng, H. A. Gasteiger and Y. Shao-Horn, *Journal of The Electrochemical

Society*, 2010, **157**, B1529.

49.   20% Platinum on Carbon XC-72 specifications, https://www.fuelcellstore.com/20-

platinum-carbon?search=20%20%%20Platinum, 2023).

50.   J. Nash, J. Zheng, Y. Wang, B. Xu and Y. Yan, *Journal of The Electrochemical

Society*, 2018, **165**, J3378.

Tables

Table 1: The FC stack operating parameters, geometric current density associated with a single cell in the FC stack (i_{Cell}), and the cathode outlet RH ($RH_{Cathode,Out}$) for the key FC systems studied.

FC system	PdMo/C-Ru$_7$Ni$_3$/C	Fe-N-C-Ni/C	PdMo/C-Ru$_7$Ni$_3$/C (30$/kW$_{Net}$)	Fe-N-C-Ni/C (30$/kW$_{Net}$)	Pt$_3$NiMo/C-Pt/C (PEMFC)
$L_{Cathode}$ (mg/cm^2)	0.0394	1.8542	0.0385	1.2193	0.0892
t_{CCL} (μm)	5.477	61.807	5.358	40.643	11.093
L_{Anode} (mg/cm^2)	0.0350	3.6206	0.0295	1.5887	0.0073
t_{ACL} (μm)	4.864	51.833	4.104	22.744	1.000
V_{Cell} (V)	0.652	0.652	0.831	0.806	0.673
P_{Inlet}^{Stack} (atm)	1.702	1.973	1.310	1.310	1.753
$RH_{Cathode,Out}$	0.759	0.874	0.686	0.687	0.884
i_{Cell} (A/cm^2)	1.763	0.670	1.949	1.551	1.912

Figures
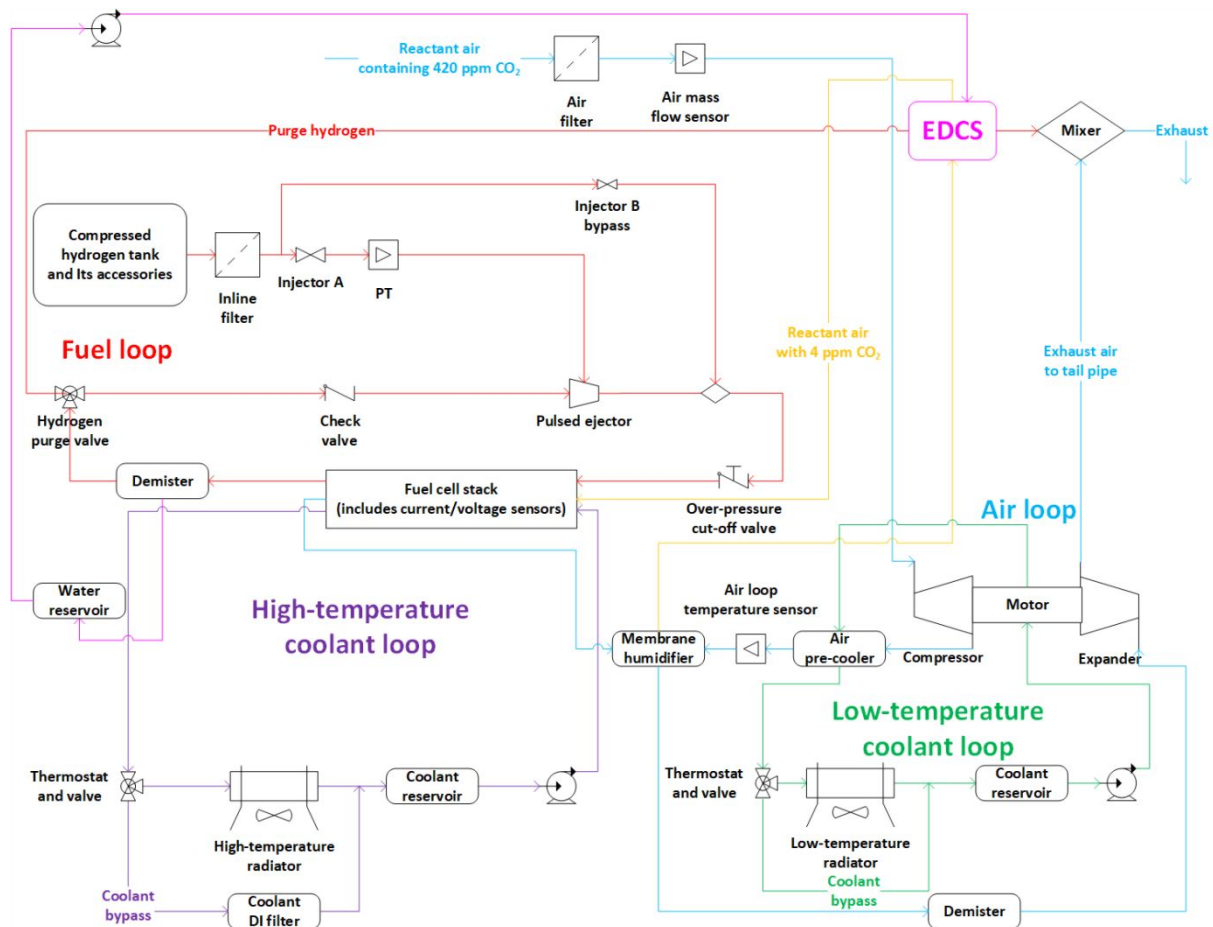
Figure 1: Schematic diagram of a comprehensive 80 kW$_{Net}$ HEMFC LDV system: FC stack and BOP, which includes an EDCS unit, an air management system (air loop), a thermal management system (high-temperature and low-temperature coolant loops), a humidification management system (membrane humidifier and air-precooler), a fuel management system (fuel loop), and additional BOP components. The HEMFC system configuration depicted in Figure 1 is the same as the 80 kW$_{Net}$ PEMFC system configuration presented in the SA report, except that we added the EDCS unit upstream of the HEMFC stack on the cathode side. The stream designated by yellow color corresponds to the humidified air stream that exits from the dry side of the membrane humidifier. This stream will go through the EDCS unit, and its CO_2 concentration will decrease from 420 ppm to 4 ppm. Based on the directions provided by DOE, we did not include the compressed H_2 tank and its accessories and the H_2 inline filter in the techno-economic analysis. PT: pressure transducer; Coolant DI filter: coolant resin deionizer filter.
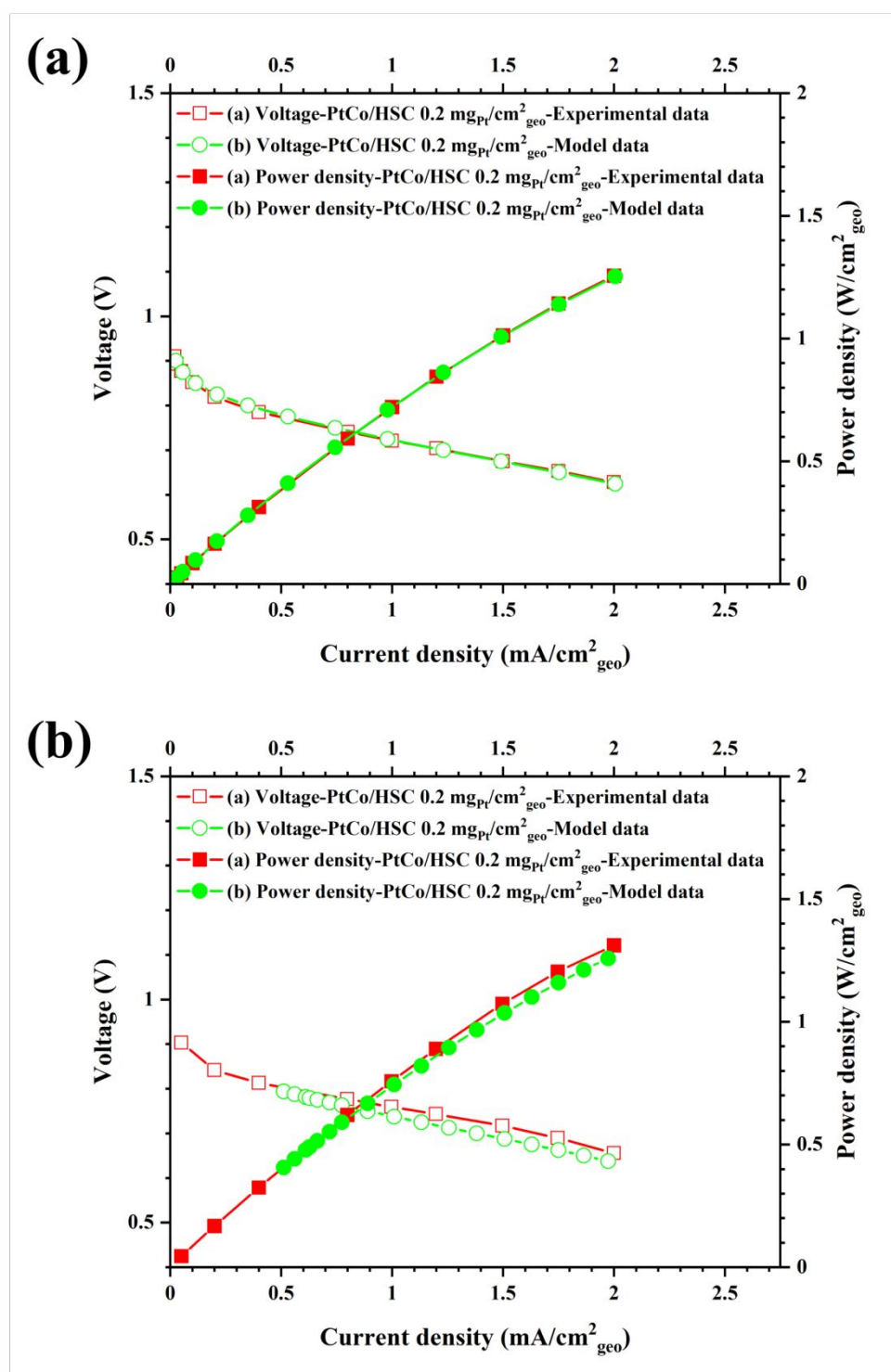
Figure 2: Comparison between model results and experimental data (a) 1-D FC sandwich model results vs. experimental data for a GM's PEMFC operating in differential mode (differential mode corresponds to high gas flows rates giving >10 H_2 and O_2 stoichiometry; 5 cm^2 active area single cell). Operating conditions of the PEMFC in the order of anode/cathode: H_2/air, 80 °C, 100/100% RH, 150/150 kPa_{Abs}. (b) Pseudo-2-D FC model results vs. experimental data for a GM's PEMFC operating in counter-flow mode (50 cm^2 active area single cell). Operating conditions of the PEMFC in the order of anode/cathode: H_2/air, 94 °C, 65/65% RH, 250/250 $kPa_{Abs,outlet}$, stoichiometries of 1.5/2.
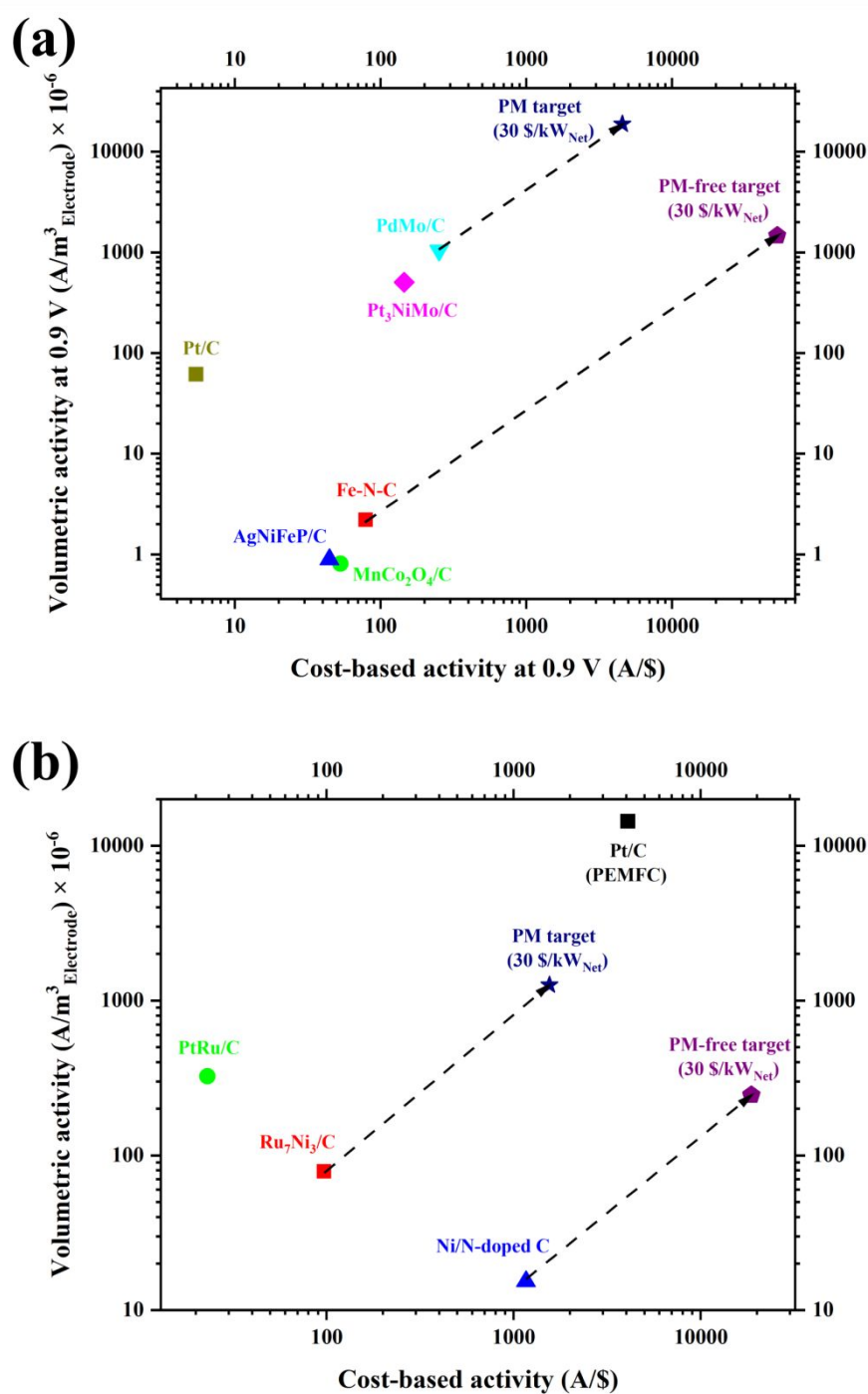
Figure 3: Comparison of the volumetric and cost-based activity of (a) ORR electrocatalysts. AgNiFeP/C (20 wt. %)[8]; Pt$_3$NiMo/C (21.63 wt. %)[47]; PdMo/C (20 wt. %)[11]; Pt/C (46 wt. %)[48]; MnCo$_2$O$_4$/C (80 wt. %)[9]; Fe-N-C[7]; (b) HOR electrocatalysts. Ru$_7$Ni$_3$/C (20 wt. %)[45]; Pt/C (20 wt. %)[40, 49]; Ni/N-doped C (83 wt. %)[10]; PtRu/C (60 wt. %)[50]. All the reported volumetric and cost-based activities are at 25 °C and 1 atm partial pressure. The arrows in the figure demonstrate how much improvement in the volumetric and cost-based activities of the ORR and HOR electrocatalysts are required to achieve the cost target of 30 $/kW$_{Net}$ for PdMo/C-Ru$_7$Ni$_3$/C and (Fe-N-C)-Ni/N-doped C HEMFC systems. For more detailed information regarding electrocatalyst properties, see Figure S2.
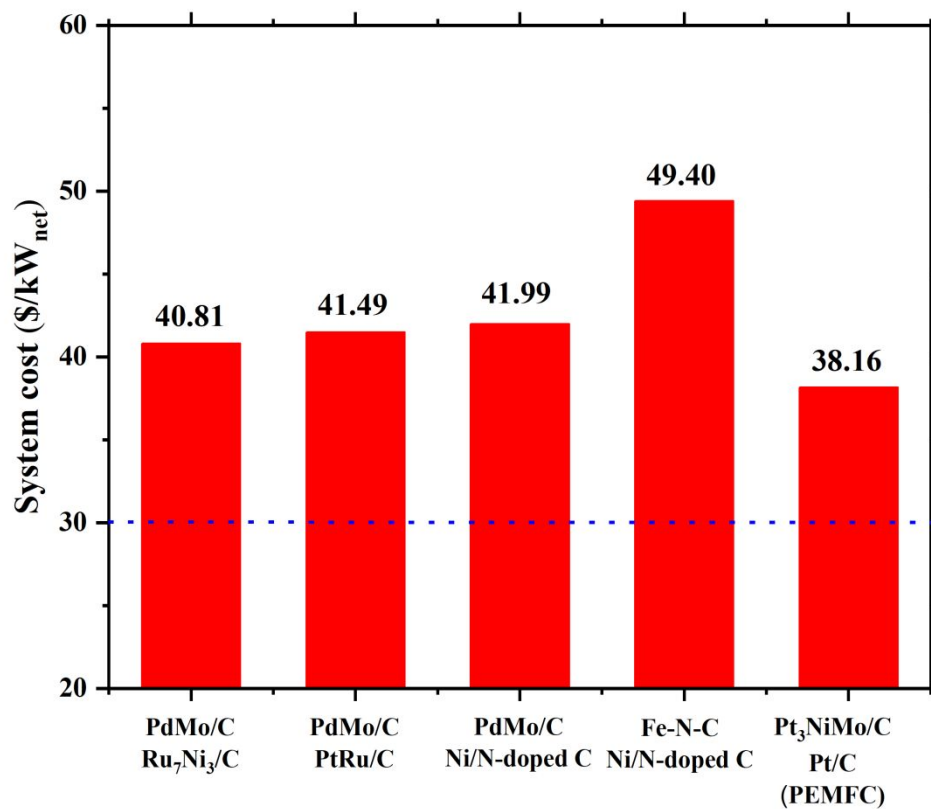
Figure 4: Comparison of 80 kW$_{Net}$ FC system cost for: 1) HEMFC systems based on judiciously selected ORR-HOR electrocatalyst pairs and 2) PEMFC system based on Pt$_3$NiMo/C-Pt/C ORR-HOR electrocatalyst pair.
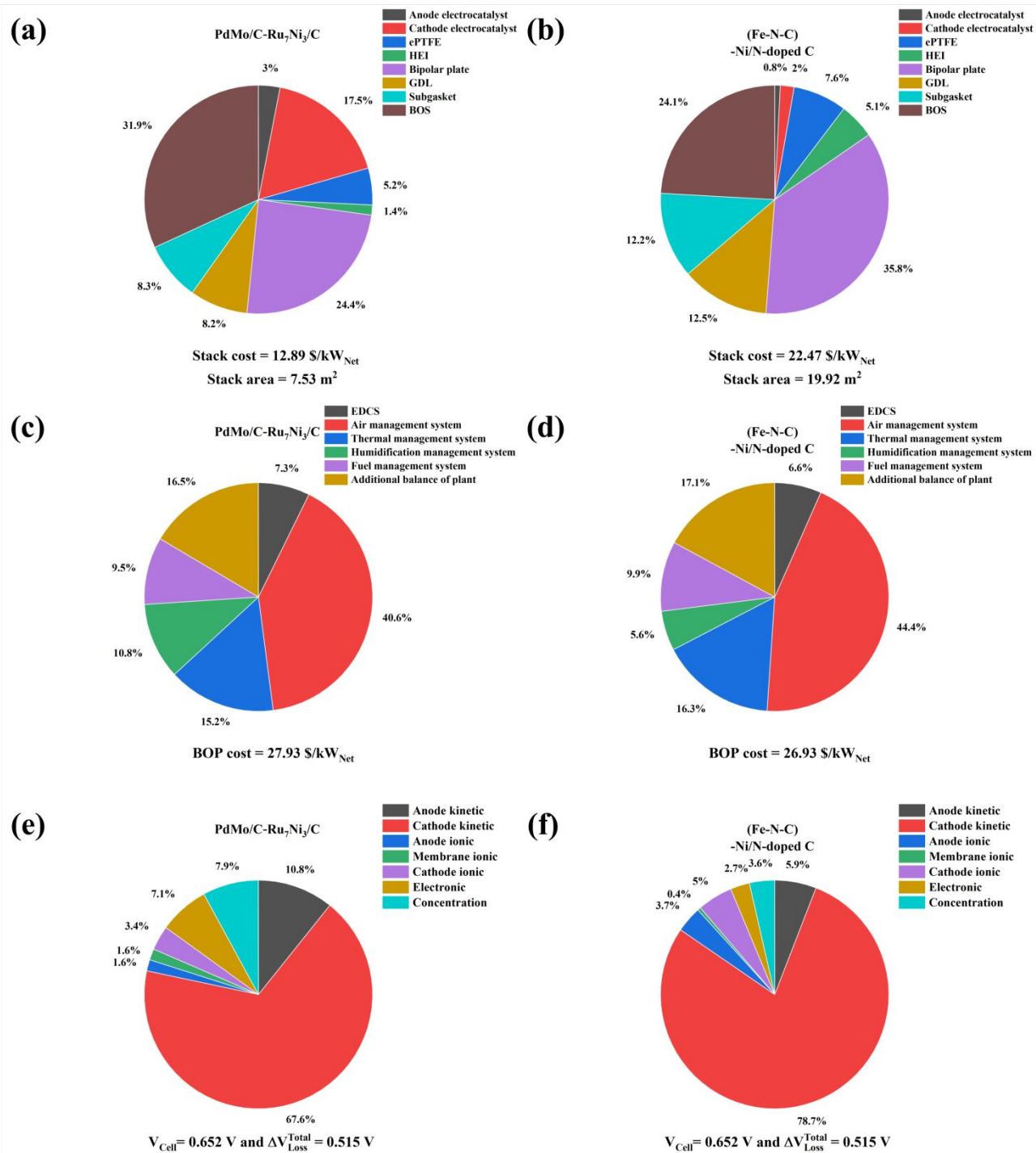
Figure 5: Cost breakdown for HEMFC stack (a) PdMo/C-Ru$_7$Ni$_3$/C and (b) (Fe-N-C)-Ni/N-doped C. Cost breakdown for HEMFC BOP (c) PdMo/C-Ru$_7$Ni$_3$/C and (d) (Fe-N-C)-Ni/N-doped C. Voltage-loss breakdown for HEMFC stack (e) PdMo/C-Ru$_7$Ni$_3$/C and (f) (Fe-N-C)-Ni/N-doped C.
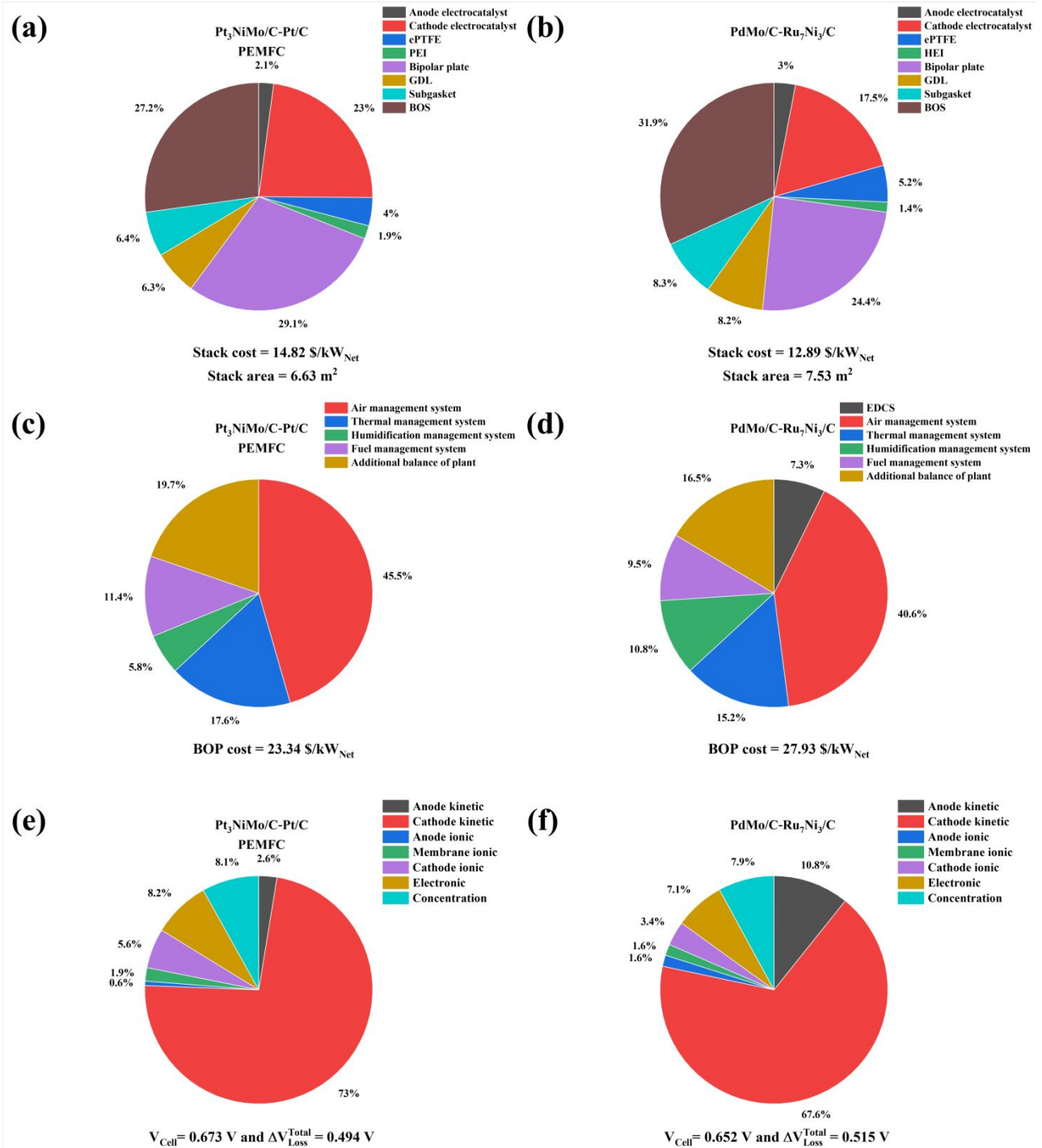
Figure 6: Stack cost breakdown for (a) Pt$_3$NiMo/C-Pt/C PEMFC system and (b) PdMo/C-Ru$_7$Ni$_3$/C HEMFC system. BOP cost breakdown for (c) Pt$_3$NiMo/C-Pt/C PEMFC system and (d) PdMo/C-Ru$_7$Ni$_3$/C HEMFC system. Voltage-loss breakdown for (e) Pt$_3$NiMo/C-Pt/C PEMFC system and (f) PdMo/C-Ru$_7$Ni$_3$/C HEMFC system.
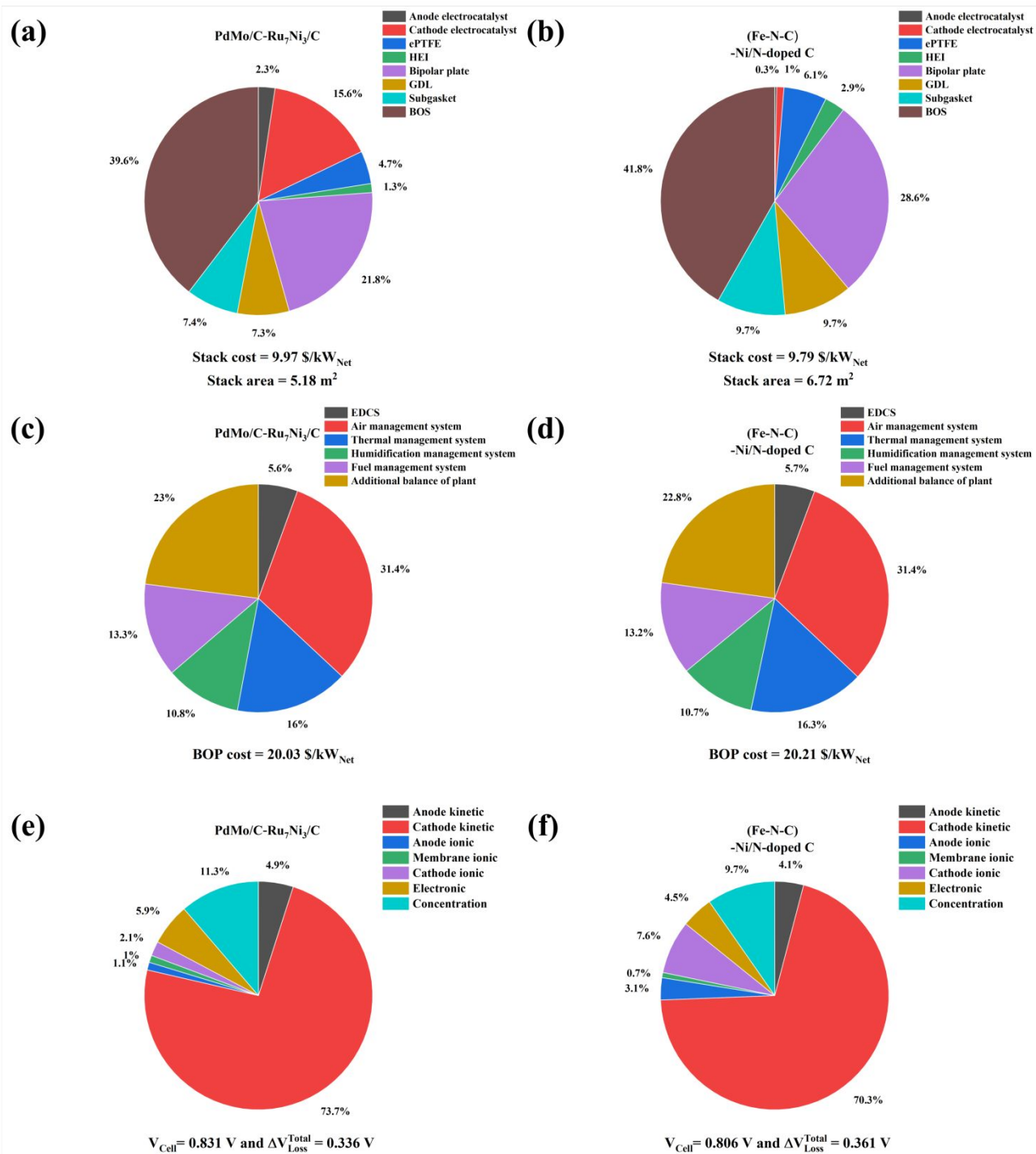
Figure 7: Stack cost breakdown for (a) 30 $/kW$_{Net}$ PdMo/C-Ru$_7$Ni$_3$/C HEMFC system and (b) 30 $/kW$_{Net}$ (Fe-N-C)-Ni/N-doped C HEMFC system. BOP cost breakdown for (c) 30 $/kW$_{Net}$ PdMo/C-Ru$_7$Ni$_3$/C HEMFC system and (d) 30 $/kW$_{Net}$ (Fe-N-C)-Ni/N-doped C HEMFC system. Voltage-loss breakdown for (e) 30 $/kW$_{Net}$ PdMo/C-Ru$_7$Ni$_3$/C HEMFC system and (f) 30 $/kW$_{Net}$ (Fe-N-C)-Ni/N-doped C HEMFC system.
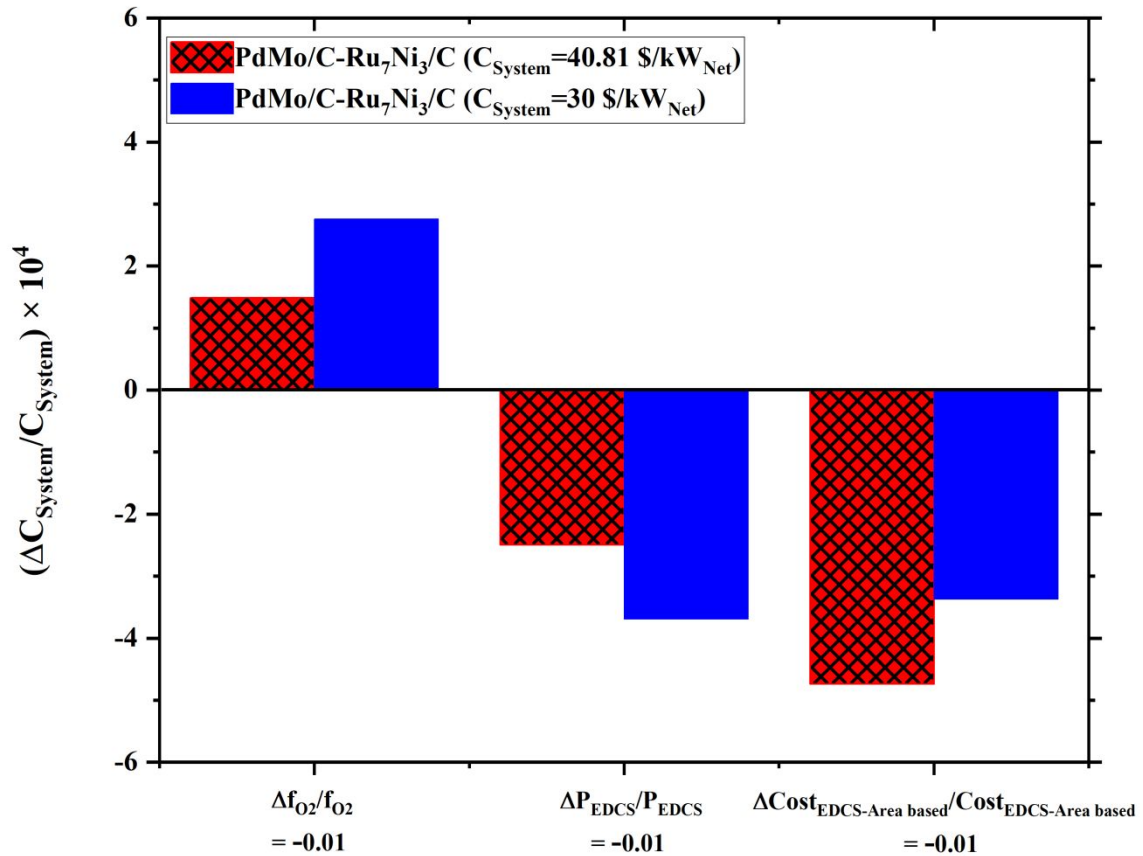
Figure 8: Single variable sensitivity analysis for the H_2 consumed to CO_2 removed ratio, ΔP_{EDCS}, and EDCS unit cost. f_{O_2} is the ratio of the molar flow rate of O_2 consumed in the EDCS unit to the molar flow rate of O_2 entering the HEMFC stack. As we showed in the ESI, f_{O_2} is linearly proportional to the H_2 consumed to CO_2 removed ratio in the EDCS unit. Therefore, we can perform the single variable sensitivity analysis of the H_2 consumed to CO_2 removed ratio by changing f_{O_2}.